COPY NO.
RM No. E6K27

NACA

RESEARCH MEMORANDUM

INVESTIGATION OF SHOCK DIFFUSERS AT MACH NUMBER 1.85

I - PROJECTING SINGLE-SHOCK CONES

By W. E. Moeckel, J. F. Connors, and A. H. Schroeder

Flight Propulsion Research Laboratory
Cleveland, Ohio

NATIONAL ADVISORY COMMITTEE
FOR AERONAUTICS

June 17, 1947
Declassified December 14, 1953

NACA RM No. E6K27

NATIONAL ADVISORY COMMITTEE FOR AERONAUTICS

RESEARCH MEMORANDUM

INVESTIGATION OF SHOCK DIFFUSERS AT MACH NUMBER 1.85

I - PROJECTING SINGLE-SHOCK CONES

By W. E. Moeckel, J. F. Connors, and A. H. Schroeder

SUMMARY

In an investigation conducted in the Cleveland 18- by 18-inch supersonic tunnel to determine design conditions for optimum performance of shock diffusers results were obtained at a Mach number of 1.85 with a series of projecting single-shock cones having angles of 20°, 30°, 40°, 50°, 60°, and 70°. Each cone was tested with a curved and with a straight diffuser-inlet section. The variation of total-pressure recovery with tip projection and outlet area was investigated for each cone to determine optimum contraction ratios and shock locations. The effect of angle of attack was also investigated for several configurations.

The maximum total-pressure recovery was obtained with the 50° cone using a straight inlet. At an angle of attack of 0°, an outlet total pressure of 92.2 percent of the free-stream value was attained. At an angle of attack of 5°, this value was reduced to 90.8 percent of the free-stream value. These total-pressure recoveries correspond to efficiencies of kinetic-energy conversion of 96.6 and 95.6 percent, respectively. Several other configurations gave total-pressure recoveries greater than 90 percent at an angle of attack of 0°.

In many tests, particularly with the larger cone angles, the total-pressure recovery in the vicinity of the maximum recovery was insensitive to changes in outlet area. The highest total-pressure recoveries were obtained with subsonic entrance flow.

INTRODUCTION

For efficient conversion of the kinetic energy of a supersonic air stream into ram pressure, the flow must be decelerated to low supersonic Mach numbers before the normal shock occurs. The deceleration may be accomplished with small total-pressure loss by contracting the flow in a converging channel or by locating one or more oblique

shocks ahead of the diffuser inlet. With the first method, the amount of deceleration allowable before the occurrence of the normal shock is limited because the normal shock will not enter the diffuser when the contraction ratio of the convergent channel is great enough to accelerate the subsonic flow behind the normal shock to sonic velocity. (See reference 1.) With the second method (that is, with a shock diffuser) no such theoretical limitation exists. The supersonic stream may be theoretically reduced to sonic velocity with negligible total-pressure loss if a sufficient number of oblique shocks of small intensity can be located ahead of the diffuser inlet.

Experiments with shock diffusers have been conducted by Oswatitsch (references 2 and 3), who determined the performance of shock diffusers having several types of projecting cone and several diffuser-inlet designs. One of these configurations yielded efficiencies greater than the theoretical maximum attainable with convergent-divergent diffusers at the same Mach numbers.

An investigation is being conducted in the Cleveland 18- by 18-inch supersonic tunnel to determine the effect on the performance of shock diffusers of varying the form of the projecting cones, the contraction ratios, and the inlet design. The results obtained with a series of single-shock cones in combination with a straight and with a curved inlet section are presented in this report. The effect of angle of attack was also investigated for several configurations.

SYMBOLS

The notation used at the shock-diffuser inlet is shown in figure 1. The symbols used in the report are defined as follows:

A	area
A_i	inlet area with cone removed
A_0/A_2	total contraction ratio
A_e/A_2	internal contraction ratio
L	tip projection, inches
M	Mach number
P	total pressure

p	static pressure
V	velocity
γ	ratio of specific heats
η	efficiency of kinetic-energy conversion
θ_c	half-angle of cone, degrees
λ	angle between flow direction and free-stream direction
ρ	density
Ψ	angle between conical ray and free-stream direction

Subscripts:

0	conditions in free stream
1	conditions immediately behind oblique shock
2	conditions at minimum flow area
3	conditions behind normal shock
4	conditions at diffuser outlet
c	conditions on cone surface
cr	critical values
e	conditions at diffuser entrance

APPARATUS AND PROCEDURE

The data presented were obtained in the Cleveland 18- by 18-inch supersonic tunnel, which was operated at a Mach number of 1.85 during the investigation. The tunnel was calibrated from measurements of the angles of oblique shocks at cone tips and from total-pressure measurements. The Mach number and total pressure in the test section measured by this method are accurate within about 2 percent. The relative total-pressure recoveries obtained in the investigation, however, are accurate within about 0.5 percent. The Reynolds number at the diffuser, based on the maximum diffuser diameter ($4\frac{1}{8}$ in.), is approximately 1.34×10^6. All pressures were photographically recorded from a multiple-tube mercury manometer. Visual and photographic observations of the flow into the diffuser inlet were made with a two-mirror schlieren apparatus.

The model used is shown in figure 2(a). The conical damper located at the rear of the cylindrical simulated combustion chamber was used to vary the outlet area of the flow through the diffuser. The pitot-static rake, located as shown in the figure, was used to obtain pressures at the diffuser outlet. During each test, these pressures were recorded for several values of the outlet area.

A section of the diffuser body showing the location of the internal support for the projecting cones is presented in figure 2(b). The cone support is faired back into the subsonic portion of the diffuser and is mounted with four struts having biconvex cross sections and a thickness ratio of 13 percent. The cone support was designed to permit instrumentation of the projecting cones; an outlet for pressure tubes from the cone is provided toward the rear of the diffuser. Because the purpose of the investigation was to determine total-pressure recoveries rather than the pressure distributions on the cone surface, no pressure tubes were installed in the support body.

The subsonic portion of the diffuser body was designed to expand the flow at a rate equivalent to a straight divergence of 5° total angle. The inlet section of the diffuser is replaceable. A straight inlet (fig. 2(c)) and a curved inlet (fig. 2(d)) were used with each cone.

The six cones used are shown in figure 3. The tip projections of the cones (distance from tip to diffuser inlet) were varied in successive steps of one-eighth inch. The theoretical location of the oblique shock relative to the two inlets is indicated for each cone at minimum tip projection. Because the angle of the air stream at the entrance lip varied with cone angle and with tip projection, a different inlet would be required for each cone at each tip projection to obtain the best possible performance. In order to expedite the determination of optimum total-pressure recoveries, however, only the inlets of figures 2(c) and 2(d) were used with each cone. With these inlets a bow wave at the diffuser entrance occurs at the minimum tip projections. Because the form and location of such a bow wave is not readily determinable, it is not shown in figure 3.

THEORY

Because the flow direction is not uniform in the field between the oblique shock and the cone surface, the theoretical flow areas A_0 and A_e and the average entrance Mach number M_e can be exactly

obtained only if the entire field is determined by an integration process. (See reference 4.) For comparison of test results with theory, the following two approximations were considered sufficiently accurate (see fig. 1):

1. The entrance Mach number M_e was assumed equal to the average of M_c and M_1, where M_c is known from conical-flow theory and M_1 is known from oblique-shock theory.

2. The approximate free-stream flow area A_0 was determined for all except the 70° cone by sketching the limiting streamline of the entering flow. The direction of the streamline at the oblique shock is known from oblique-shock theory. In order to determine the direction at other points, a linear variation of the flow angle λ with the angle Ψ of a ray from the cone tip was assumed in the region between the shock and the cone surface.

For the 70° cone, M_c is equal to 0.94 and M_1 is 1.05; hence, M_e is less than 1.0. Because there is spillage of the flow around the entrance lip when M_e is subsonic, the method described for determining A_0 is justified only if M_e is greater than 1.0. For the 70° cone an alternative method, using the constant-mass-flow relation, was therefore used to determine A_0:

$$\frac{A_0}{A_e} = \left[\frac{\dfrac{(\rho V)_e}{(\rho V)_{e,cr}}}{\dfrac{(\rho V)_0}{(\rho V)_{0,cr}}} \right] \frac{P_e}{P_0} \qquad (1)$$

where the ratios $(\rho V)/(\rho V)_{cr}$ are the reciprocal of the contraction ratios required to isentropically lower the local Mach number to unity. Because M_e is nearly equal to 1.0 for the 70° cone, $(\rho V)_e/(\rho V)_{e,cr}$ was assumed equal to 1.0. For an M_0 of 1.85, $(\rho V)_0/(\rho V)_{0,cr}$ is equal to 0.669 and P_e/P_0 is equal to 0.90. Hence, for the 70° cone, $A_0 = 1.345\ A_e$.

A sufficiently close approximation for A_e was obtained by assuming that the flow at the inlet is parallel to the cone surface. (See fig. 1.) This assumption gives the minimum possible area for the entrance flow. (The actual minimum A_e is given by a catenary curve, but the difference between this value and the area normal to

the cone surface was found to be negligible.) The maximum error resulting from this approximation was determined by comparing the resulting A_e with the upper limit for this value (A_e perpendicular to the free-stream direction). For the most unfavorable case (60° cone, L = 0.8 in.) the difference between the lower limit and the upper limit was about 6 percent. For smaller cone angles, the maximum error was considerably less. Inasmuch as the flow at the cone surface is known to be parallel to that surface, the lower limit should be much nearer the real value than the upper limit. The variation of A_e/A_2 with tip projection is shown for each cone-inlet combination in figure 4.

Two flow conditions must be distinguished in determining the theoretical variation of P_4 with A_4. These conditions will be designated the supercritical and the subcritical. In the supercritical-flow region, the mass flow through the diffuser remains constant as A_4 is varied. For this region the theoretical curve of total-pressure recovery against outlet area is given by the equation:

$$\frac{P_4 A_4}{P_0 A_i} = \frac{(\rho V)_0}{(\rho V)_{0,cr}} \frac{A_0}{A_i} \tag{2}$$

In the subcritical region, the normal shock stands outside the diffuser inlet and the mass flow varies with changes in outlet area. The theoretical total-pressure recovery under these conditions may be calculated if the flow ahead of the normal shock is assumed to remain unaffected as the normal shock moves outward and if any losses resulting from spillage of the entrance flow are neglected. With these assumptions, the theoretical recovery remains constant as A_4 is varied and is equal to the product of the total-pressure ratios across the oblique and across the normal shock. In the calculation of this total-pressure recovery for comparison with test data, the normal shock was assumed to occur at the Mach number M_e. As the angle of the projecting cones increases, M_e decreases and the total-pressure loss across the normal shock thus decreases. The total-pressure loss across the oblique shock, however, increases with cone angle. An optimum cone angle should therefore exist for high efficiencies in the subcritical region.

The value of A_4 for which transition from supercritical to subcritical flow takes place was calculated as follows: If the contraction ratio A_e/A_2 is sufficiently small, the normal shock

is located inside the diffuser past the minimum area for values of A_4 in the supercritical region. When the flow area at the location of the normal shock is equal to A_e, the normal shock occurs at a Mach number M_e, as previously determined. As A_4 is decreased, the normal shock advances toward the diffuser inlet. The critical A_4 is obtained when the normal shock is at the minimum area A_2. The Mach number at this minimum area is determined from A_e/A_2. The critical value of A_4/A_i may then be determined from equation (1); P_4/P_0 is taken equal to the product of the total-pressure ratios across the oblique shock and across the normal shock that occurs at Mach number M_2. When M_e is subsonic, as with the 70° cone, only the total-pressure ratio across the oblique shock was considered.

The preceding analysis is based on the assumption that the inlets are so designed that the normal shock will pass into the diffuser when A_4/A_i is in the supercritical region. If the normal shock is forced to remain ahead of the inlet, either because the angle of deflection at the inlet is too great or because the internal contraction ratio is too great, then A_0 is less than the theoretically determined values because the flow spills around the entrance lip. An estimate of the conditions for which the normal shock remains outside the diffuser for the inlets actually used showed that, for the straight inlet, an external bow wave would occur for the large-angle cones. For these cones, however, the inlet Mach number is sufficiently small that little advantage may be expected from internal contraction. With the curved inlet, on the other hand, an external bow wave was to be expected for nearly all cones and tip projections, but the angle of the entrance lip provides a closer approximation to the actual entrance-flow direction with large-angle cones than the straight inlet. Furthermore, because the minimum area occurs at the inlet for most tip projections with this inlet, a normal shock at the entrance was desirable for optimum total-pressure recovery.

Thus, the reasons for the choice of these two inlets are as follows: The straight inlet provided a means of testing the effect of internal contraction ratio for those cones for which internal contraction is most beneficial (small-angle cones). The curved inlet, on the other hand, corresponded for most tip projections to a shock diffuser with no internal contraction. For the large-angle cones, furthermore, the curved inlet provided a means of determining the advantage of providing a smooth entrance flow when the normal shock occurs at the inlet.

Neither of the inlets was designed to allow entry of the oblique shocks into the diffuser. With the straight inlet, the total-flow contraction becomes greater than the isentropic contraction ratio from the free-stream Mach number to unity unless the oblique shock is somewhat ahead of the entrance lip. For the curved inlet, as previously stated, the angle of the entrance lip results in a bow wave for most cones and tip projections.

RESULTS

For each cone-inlet combination the total-pressure recovery was determined as a function of outlet-inlet area ratio for several tip projections at an angle of attack of 0°. The effect of angle of attack and the distribution of the pressures at the diffuser outlet were also determined for the configurations giving the highest total-pressure recoveries. The experimental results are compared with theoretical calculations, and schlieren photographs of typical flow patterns are presented.

Variation of total-pressure recovery with outlet area. - The experimental data points are presented in figure 5 for each of the configurations tested; the total-pressure recovery P_4/P_0 is plotted against outlet-inlet area ratio A_4/A_i rather than against A_4/A_0 because A_i is a geometrical constant for each inlet, whereas A_0 is an approximation. The theoretically computed variation of P_4/P_0 with A_4/A_i is included for comparison. The theoretical critical area ratio $(A_4/A_i)_{cr}$ is given in each case by the upper limit of the supercritical portion of the theoretical curves. The subcritical theoretical lines are dashed to indicate that the assumptions used to calculate them are incomplete. The fact that most of the data points in the supercritical region fall to the right of the theoretical curves is to be expected because any boundary-layer build-up at the diffuser outlet tends to make the flow area less than the measured geometrical area. Any total-temperature losses in the subsonic portion of the diffuser would also tend to make P_4/P_0 for a given A_4/A_i greater than the theoretically predicted values. In the tests for which data points fell very close to, or to the left of, the theoretical curves, the normal shock remained outside the diffuser inlet during the entire run. Under these conditions some of the flow spills around the diffuser entrance lip, and consequently the actual A_0 becomes less than the theoretically calculated value. (See figs. 5(c), 5(e), 5(g), and 5(i).)

In agreement with theoretical predictions, the subcritical total-pressure recoveries vary with cone angle. For most of the configurations,

P_4/P_0 decreases with A_4/A_i in this region, which indicates that the subcritical flow is more complicated than assumed. This decrease of P_4/P_0, however, becomes less as the cone angle increases. With the 50° and 60° cones (figs. 5(g), 5(h), 5(i), and 5(j)), a high pressure recovery is maintained throughout the subcritical region for some tip projections. It should also be noted that in the vicinity of the maximum total-pressure recovery, P_4/P_0 becomes less sensitive to variation in A_4/A_i as the cone angle increases. Schlieren observations showed that for the 60° cone the highest total-pressure recoveries were obtained with subcritical inlet flow.

The maximum total-pressure recovery ($P_4/P_0 = 0.922$) was obtained with the 50° cone, using the straight inlet and a tip projection of 1.25 inches (fig. 5(g)). With the curved inlet, the best recovery ($P_4/P_0 = 0.917$) was obtained with the 60° cone at a tip projection of 0.925 inch (fig. 5(j)). These recoveries correspond to efficiencies of kinetic-energy conversion of 96.6 and 96.4 percent, respectively. These experimental efficiencies are greater than the maximum theoretically obtainable (95.5 percent) with a convergent-divergent diffuser designed to allow entry of the normal shock. The maximum experimental efficiency yet reported with a convergent-divergent diffuser is 92.5 percent ($P_4/P_0 = 0.839$). (See reference 5.) The relation between P_4/P_0 and η, as defined in reference 1, is given in the notation of this paper by the equation

$$\eta = 1 - \frac{2}{(\gamma-1)\,M_0^2}\left[\left(\frac{P_0}{P_4}\right)^{\frac{\gamma-1}{\gamma}} - 1\right] \qquad (3)$$

Effect of angle of attack. - The effect of angle of attack on the total-pressure recoveries for the three best configurations is shown in figure 6. When the angle of attack was increased to 5°, the maximum total-pressure ratio dropped from 0.922 to 0.908 for the 50° cone with the straight inlet (fig. 6(a)). With the curved inlet, the maximum total-pressure ratio dropped from 0.913 to 0.863 for the 50° cone and from 0.914 to 0.875 for the 60° cone (figs. 6(b) and 6(c), respectively). These results confirm those of Oswatitsch (reference 2), who found that the effect of angle of attack was small for the shock diffuser that he investigated.

Pressure distribution at diffuser outlet. - In figure 7, the total-and static-pressure distribution at the inlet of the simulated combustion chamber is plotted for the configuration giving the maximum

total-pressure recovery. (See fig. 5(g).) The static-pressure distribution (fig. 7(a)) is uniform. The total-pressure distribution plotted in figure 7(b) is therefore an indication of the velocity distribution at the combustion-chamber inlet. This velocity distribution is seen to be satisfactory for values of A_4/A_i near the critical value. For greater values of A_4/A_i, the presence of the outlet for the pressure tubes (fig. 2(b)) apparently disturbed the regularity of the flow. In the region of interest (near the critical A_4/A_i) the presence of the central cone, its support body, the supporting struts, and the pressure-tube outlet had no serious effect on the regularity of the velocity distribution.

Typical inlet flow patterns. - Some typical flow patterns observed with schlieren photographs for various cone-inlet combinations are shown in figure 8. Figure 8(a) is a photograph of a typical schlieren pattern obtained when the total contraction ratio was too great. There is some spillage of the flow, although A_4/A_i is far in the supercritical region. The double image of the oblique shock indicates that a vibration of the shock pattern may be taking place. This photograph was obtained for a test using the 30° cone with a straight inlet, a tip projection of 1.55 inches, and an angle of attack of 0°. (See fig. 5(c).) The disturbances on the outside of the diffuser body arise from the pressure tubes used for determining internal pressure distribution. These tubes were not used in the tests.

The types of flow pattern obtained in the subcritical region and in the supercritical region with optimum tip projections are shown in figures 8(b) and 8(c), respectively. The configuration shown is the 40° cone with the straight inlet, a tip projection of 1.50 inches, and an angle of attack of 0°. With subcritical flow (fig. 8(b)) a somewhat complicated shock pattern is obtained, and there is some spillage of the flow around the entrance lip. The faint dark line parallel to the diffuser inlet is the projection of the bow wave and should not be interpreted as an additional shock. The total-pressure recovery for this condition is only slightly less than the maximum obtained at this tip projection. (See fig 5(e).) The supercritical flow pattern for the same configuration is shown in figure 8(c). The bow wave now curves toward the inside of the diffuser. The narrow dark strip at the diffuser inlet again does not indicate an external normal shock, but is the projection of the three-dimensional bow wave. A second oblique shock appeared to be present in the field between the cone tip and the diffuser inlet. Such shocks probably result from boundary-layer build-up and have a beneficial effect on total-pressure recovery. Oswatitsch found that the maximum total-pressure recovery of his shock diffusers was slightly decreased when boundary-layer suction was employed (reference 2).

The flow pattern at an angle of attack of 5° is shown in figure 8(d) for the configuration that yielded the highest total-pressure recovery in the present investigation. (See fig. 5(g).) Again, as in figure 8(b), a faint dark line, which is the projection of the bow wave, appears ahead of the inlet. That a considerable portion of the entrance flow is subsonic may be deduced from the spillage around the entrance lip. A separation of the boundary layer is visible on the upper surface of the cone.

The flow patterns corresponding to the best total-pressure recovery obtained with the 60° cone are shown in figures 8(e) and 8(f). The configuration in figure 8(e) is the straight inlet with tip projection of 0.925 inch. With the same cone but with curved inlet, the best recovery was obtained with the flow pattern shown in figure 8(f). The data for these two tests are plotted in figures 5(i) and 5(j), respectively. These photographs, together with figure 8(d), show that the best recoveries with the 50° and 60° cones were obtained with subcritical flow.

Variation of maximum total-pressure recovery with tip projection and contraction ratios. - Maximum total-pressure recoveries obtained with the straight and the curved inlet are plotted in figure 9 against tip projection, total contraction ratio, and internal contraction ratio for each of the cones tested. For the 20° cone (fig. 9(a)) the optimum tip projection occurs for the straight inlet at 2.875 inches, corresponding to a total contraction ratio $A_0/A_2 = 1.37$ and an internal contraction ratio $A_e/A_2 = 1.195$. With the curved inlet the optimum point was not determinable because the minimum tip projection attainable was 2.5 inches. The data points indicate, however, that the maximum P_4/P_0 would fall below that obtained with the straight inlet. An examination of the schlieren photographs for the straight-inlet tests showed that the normal shock remained outside the diffuser inlet for tip projections less than 2.875 inches; consequently, lower total-pressure recoveries were obtained.

The variation of maximum P_4/P_0 with tip projection and contraction ratio is similar for each of the cones tested. The maximum P_4/P_0 drops quite rapidly as the tip projection is decreased or increased from optimum. When M_e is supersonic, the decrease in P_4/P_0 with tip projections greater than optimum (A_e/A_2 less than optimum) is to be expected, because the normal shock occurs at a higher Mach number as A_e/A_2 decreases. For tip projections less than optimum the maximum P_4/P_0 is probably lower because the normal shock remains outside the diffuser entrance. With the 70° cone, however, M_e is already subsonic, and the bow wave does not extend

into the subsonic region. For this cone, therefore, the reasons for the decrease in total-pressure recovery for tip projections less than and greater than optimum are less obvious.

The maximum P_4/P_0 at optimum tip projection is greater for the straight than for the curved inlet for all except the 60° and 70° cones (fig. 9). For the 50° and 60° cones (figs. 9(d) and 9(e)) total-pressure recoveries above 90 percent were obtained with the straight and with the curved inlet.

ANALYSIS OF RESULTS

The maximum total-pressure recovery through a series of oblique shocks followed by one normal shock was determined theoretically by Oswatitsch (reference 2) for a range of Mach numbers from 1 to 4. He found that the optimum recovery through such a series of shocks was obtained when the static-pressure ratio was the same across each shock. Theoretical recoveries higher than the values calculated by Oswatitsch are possible with a shock diffuser employing conical projections. The isentropic compressions between the shock and the cone surface and from the inlet to the minimum internal area, not considered by Oswatitsch, tend to lower the Mach number at which the normal shock takes place and hence tend to raise the maximum total-pressure recovery.

In the notation of figure 1, the assumptions made by Oswatitsch correspond to a shock diffuser with minimum cross section at A_e and with $M_e = M_1$. Theoretical curves based on the assumption that A_e/A_2 is equal to the maximum allowable contraction ratio for a Mach number of M_e, according to one-dimensional-flow theory, are plotted in figures 10 and 11. Because M_e is not uniform at the inlet, two curves were calculated: The solid and dashed curves correspond to the assumptions that $M_e = M_c$ and $M_e = M_1$, respectively. Because the average M_e lies between these two extremes, the theoretical maximum recoveries should lie between the dashed and solid curves. In figure 10 the theoretical recoveries are plotted against cone angle for various Mach numbers. The maximum theoretical recoveries are obtained with cone angles of about 50° for Mach numbers greater than 2.0. In figure 11 the maximum recoveries from figure 10 are plotted as functions of free-stream Mach number. The curve obtained by Oswatitsch is included for comparison.

The experimental maximum total-pressure recoveries obtained with each of the cones are compared with the theoretical maximum values in figure 12, and the internal contraction ratios for which these recoveries were obtained are compared with the maximum theoretical contraction

ratios given by one-dimensional theory. For the straight inlet, the experimentally determined optimum contraction ratios lie quite close to the theoretical curves except for that of the 30° cone, for which the optimum contraction ratio is considerably above the theoretical maximum. The reason for this excessive optimum contraction ratio is unknown.

The variation of the maximum total-pressure recoveries with cone angle for the straight inlet is similar to the theoretical variation, although the data points are from 2 to 8 percent below the higher theoretical curve. Some of this difference may be attributed to total-pressure losses in the subsonic part of the diffuser. The high recovery obtained with the 20° cone with straight inlet is probably due to the additional oblique shock from the entrance lip toward the interior. This additional shock should be especially valuable with small cone angles for which M_e is still fairly large. It should be noted that the 30° cone, whose optimum contraction ratio is considerably above the theoretical value, yields a maximum total-pressure recovery somewhat low in comparison with the recovery obtained with the 20° cone.

With the straight inlet, the 20°, 30°, and 40° cones gave maximum values of P_4/P_0 at values of A_e/A_2 greater than the maximum theoretical values (fig. 12). This discrepancy cannot be explained by assuming an error in the approximation of A_e for these cones because this approximation is very close to the minimum possible value. For the 60° cone, on the other hand, the optimum contraction ratio is slightly less than the theoretical maximum contraction ratio. With this particular configuration, the maximum recovery occurred with subcritical flow (fig. 5(i)) for which an optimum value of A_e/A_2 of 1.0 is to be expected.

With the curved inlet the optimum contraction ratio was below the theoretical maximum for all cones tested because, for larger contraction ratios (smaller tip projections), the oblique shocks did not pass outside the entrance lip and consequently a bow wave formed ahead of the diffuser inlet for the reason previously stated. The maximum total-pressure recovery (fig. 12) was below that obtained with the straight inlet for all except the 60° and the 70° cones. With these two cones, the highest recoveries were obtained with subsonic entrance flow for which internal contraction ratios less than 1.0 (expansions) are not harmful. (The points for the 20° cone with the curved inlet should be disregarded because no optimum values were obtained for this configuration, fig. 9(a).)

For the straight inlet, therefore, the condition for optimum tip projection is that the internal contraction ratio must be

approximately equal to the maximum theoretical contraction ratio which will permit a normal shock at Mach number M_e to enter the diffuser inlet. For the curved inlet, the condition is that the oblique shock must pass just outside the entrance lip. The extent to which these conditions apply may be seen from the following table:

Cone (deg)	Inlet	Minimum tip projection for external oblique shock (in.)	Tip projection for maximum theoretical A_e/A_2 ($M_e = M_1$) (in.)	Experimental tip projection for maximum P_4/P_0 (in.)
20	Straight	1.66	2.94	2.875
30	---do---	1.52	1.99	1.80
40	---do---	1.28	1.52	1.50
50	---do---	1.08	1.22	1.25
60	---do---	.88	.98	1.175
20	Curved	1.50	1.80	Not determined
30	---do---	1.38	1.14	1.55
40	---do---	1.16	.93	1.25
50	---do---	.98	.81	1.125
60	---do---	.80	.65	.925

Because for the configurations with the straight inlet the oblique shock was outside before the maximum theoretical internal contraction was reached, only the contraction-ratio condition is significant.

The optimum tip projection was determined for the curved inlet by the condition that the oblique shock must pass outside the entrance lip. The lower total-pressure recoveries obtained with the curved inlet for the 20°, 30°, 40°, and 50° cones are probably due to the limitation in internal contraction ratio imposed by the oblique-shock condition. There is no reason to suppose that these recoveries could not be raised to values obtained with the straight inlet by altering the geometry of the curved inlet to give optimum internal contraction while an external oblique shock is maintained. Inasmuch as the total-pressure recoveries for the 60° and the 70° cones were greater for the curved than for the straight inlet, a smooth turning of the flow may be of some advantage, at any rate for subsonic entrance flow.

SUMMARY OF RESULTS

An investigation in the Cleveland 18- by 18-inch supersonic tunnel of the total-pressure recovery obtainable with shock diffusers that have single-shock projecting cones gave the following results:

1. The maximum total-pressure recovery was obtained with a 50° cone in combination with a straight inlet. At an angle of attack of 0°, an outlet total pressure of 92.2 percent of the free-stream value was attained with this configuration. At an angle of attack of 5°, this value was reduced to 90.8 percent of the free-stream value. These total-pressure recoveries correspond to efficiencies of kinetic-energy conversion of 96.6 and 95.6 percent, respectively. Several other configurations at an angle of attack of 0° yielded total-pressure recoveries greater than 90 percent (efficiencies greater than 95.5 percent). (The maximum theoretical total-pressure recovery for a convergent-divergent diffuser is 89 percent, whereas the maximum experimental recovery thus far attained is 83.9 percent (efficiency, 92.5 precent).)

2. These maximum recoveries were obtained with subsonic entrance flow and high recoveries were maintained throughout the subcritical region with the 50° and 60° cones.

3. An optimum tip projection was found for each cone-inlet combination tested. With external oblique shocks, this optimum tip projection occurred when the internal contraction ratio was approximately equal to the maximum theoretical contraction ratio allowable to permit entry of a normal shock at the entrance Mach number.

4. The variation of maximum total-pressure recovery with cone angle was found to be in approximate agreement with theoretical predictions.

Flight Proplusion Research Laboratory,
National Advisory Committee for Aeronautics,
Cleveland, Ohio.

REFERENCES

1. Kantrowitz, Arthur, and Donaldson, Coleman, duP.: Preliminary Investigation of Supersonic Diffusers. NACA ACR No. L5D20, 1945.

2. Oswatitsch, Kl.: Der Druckrückgewinn bei Geschossen mit Rückstossantrieb bei hohen Überschallgeschwindigkeiten (Der Wirkungsgrad von Stossdiffusoren). Bericht Nr. 1005, Forschungen und Entwicklungen des Heereswaffenamtes, Kaiser Wilhelm-Inst. f. Stromungsforschung, Gottingen, Jan. 1944. (The Pressure Recovery of Projectiles with Jet Propulsion at High Supersonic Speeds (The Efficiency of Thrust Diffusors).) Trans. By Douglas Aircraft Co., Inc., 1946.

3. Oswatitsch, Kl., and Böhm, H.: Luftkrafte und Stromungsvorgange bei angetriebenen Geschossen. Bericht Nr. 1010, Nr. 1010/2, Forschungen und Entwicklungen des Heereswaffenamtes, Kaiser Wilhelm-Inst. f. Stromungsforschung, Gottingen, Aug., Oct. 1944. (Air Forces and Flow Phenomena on Propelled Projectiles. Trans. by Douglas Aircraft Co., Inc., Feb. 14, 1946.)

4. Taylor, G. I., and Maccoll, J. W.: The Air Pressure on a Cone Moving at High Speeds. - I and II. Proc. Roy. Soc. (London), ser. A, vol. 139, no 838, Feb. 1, 1933, pp. 278-311.

5. Wyatt, DeMarquis D., and Hunczak, Henry R.: An Investigation of Convergent-Divergent Diffusers at Mach Number 1.85. NACA RM No. E6K21, 1947.

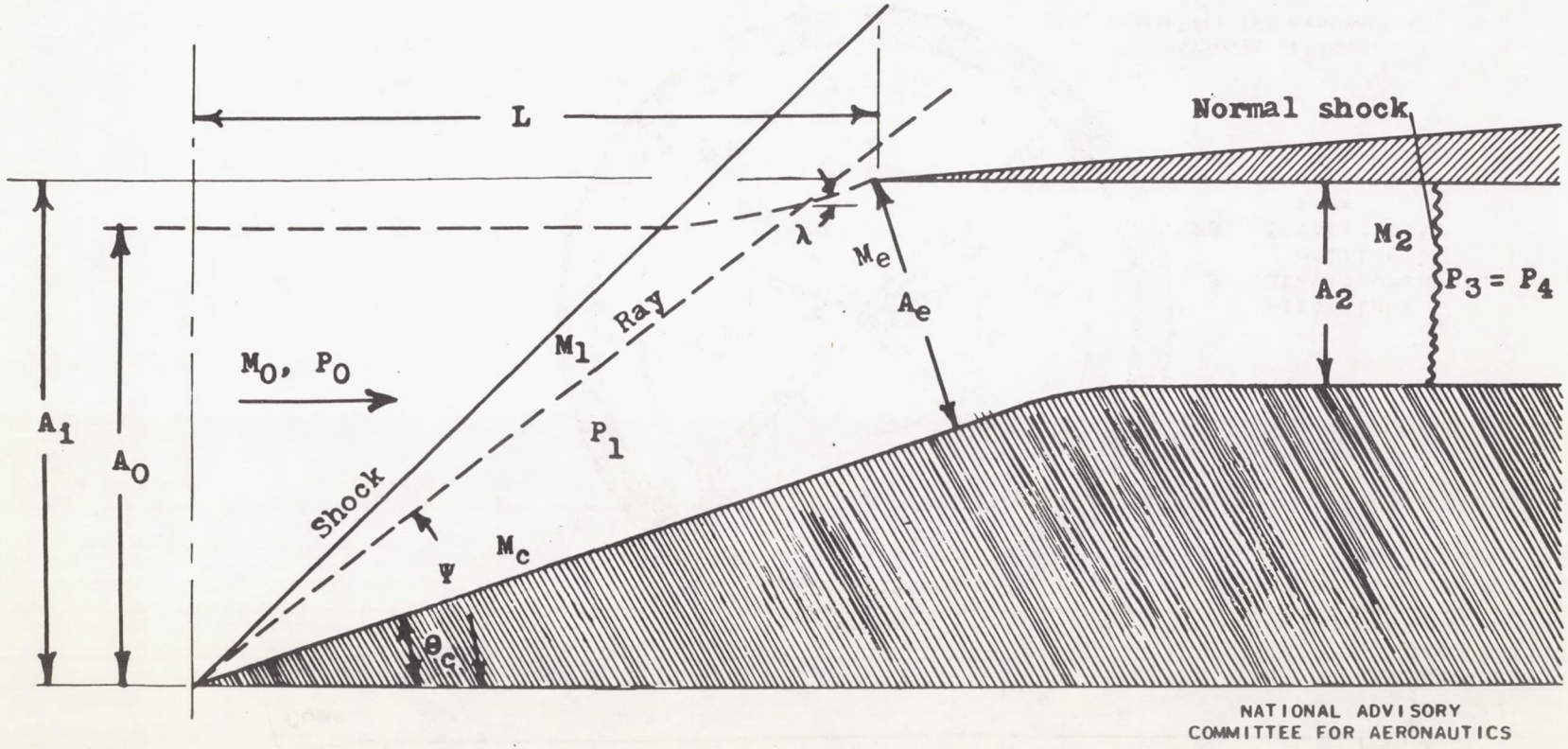

Figure 1.- Notation used at shock-diffuser inlet.

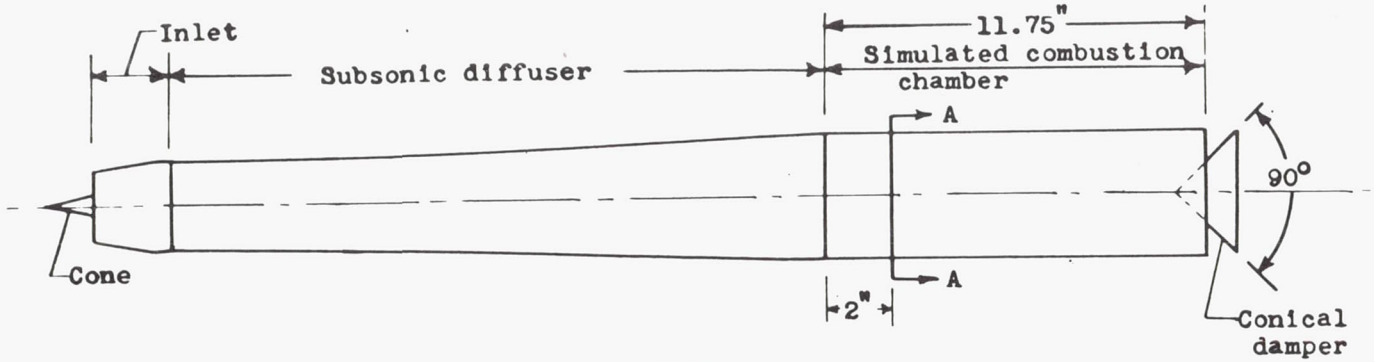

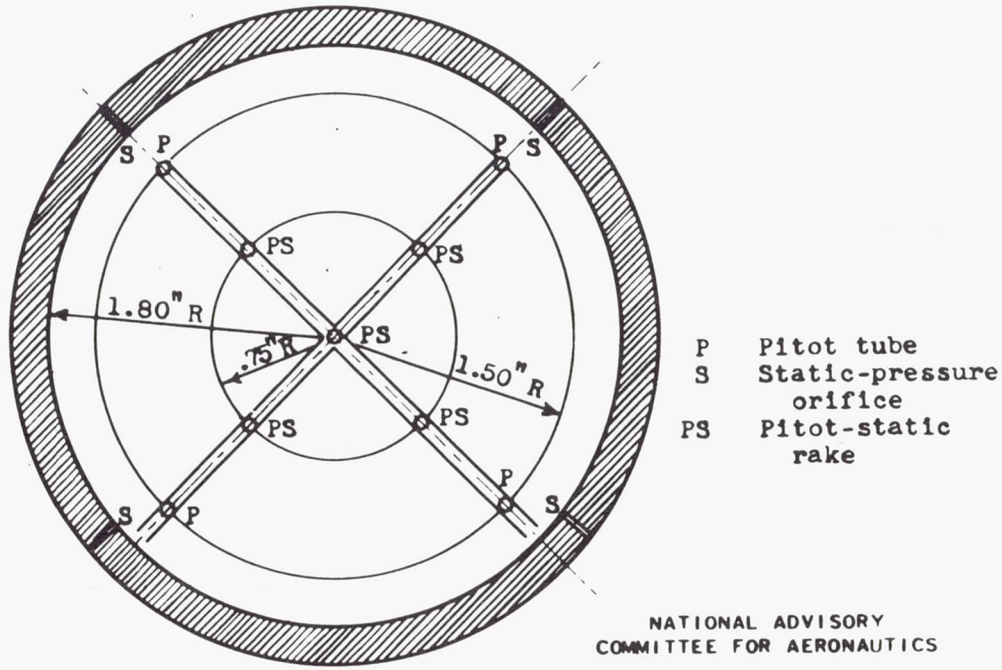

Section A-A

(a) Schematic drawing of diffuser and simulated combustion chamber showing pressure instrumentation.

Figure 2.- Experimental model.

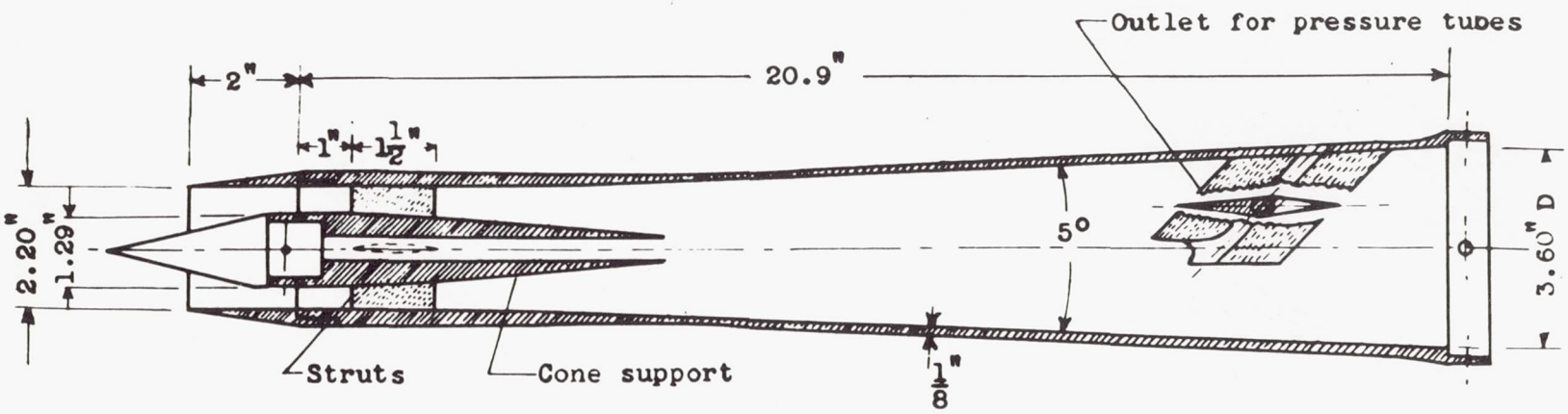

(b) Diffuser body and cone support.

NATIONAL ADVISORY
COMMITTEE FOR AERONAUTICS

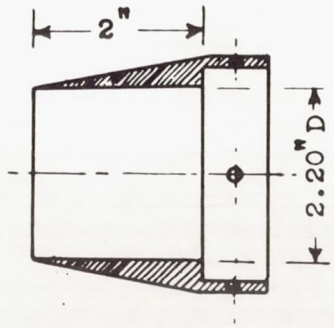

(c) Straight inlet.

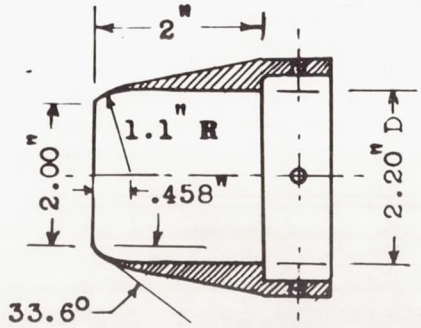

(d) Curved inlet.

Figure 2.- Concluded. Experimental model.

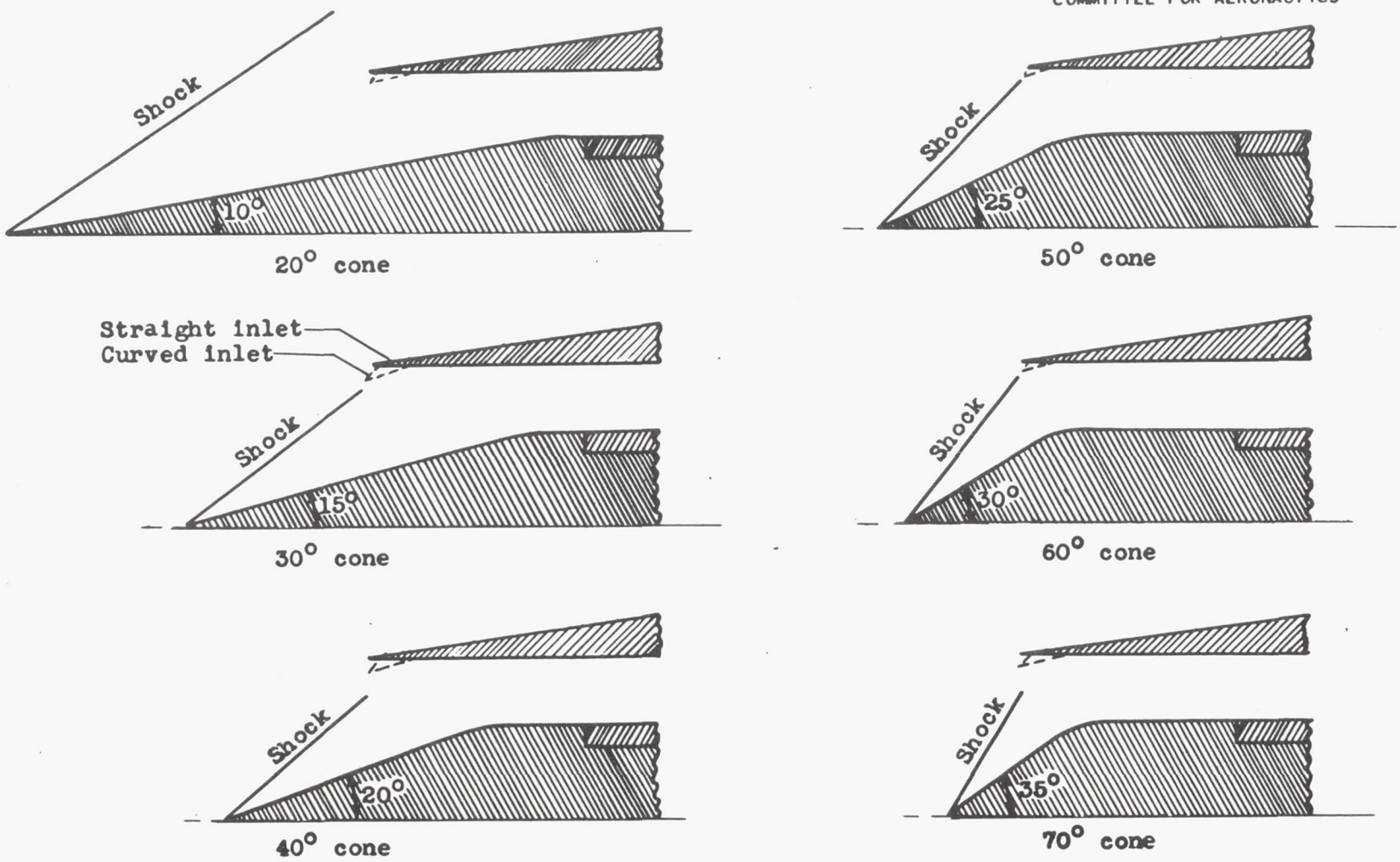

Figure 3.- Sketches of cones showing theoretical oblique-shock positions for minimum tip projections. (Bow wave at inlet not shown.)

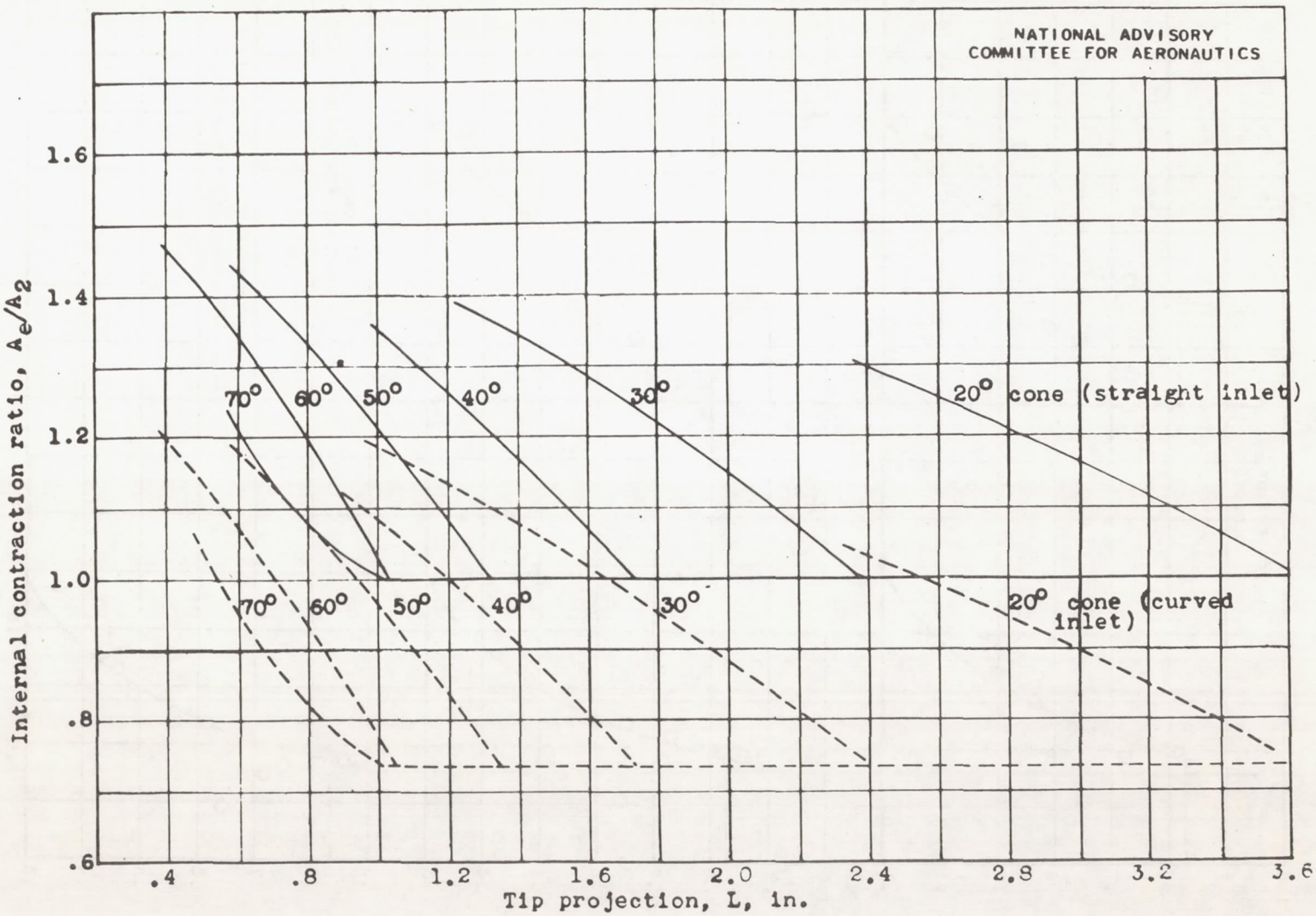

Figure 4.- Variation of calculated internal contraction ratio with tip projection for cones of figure 3.

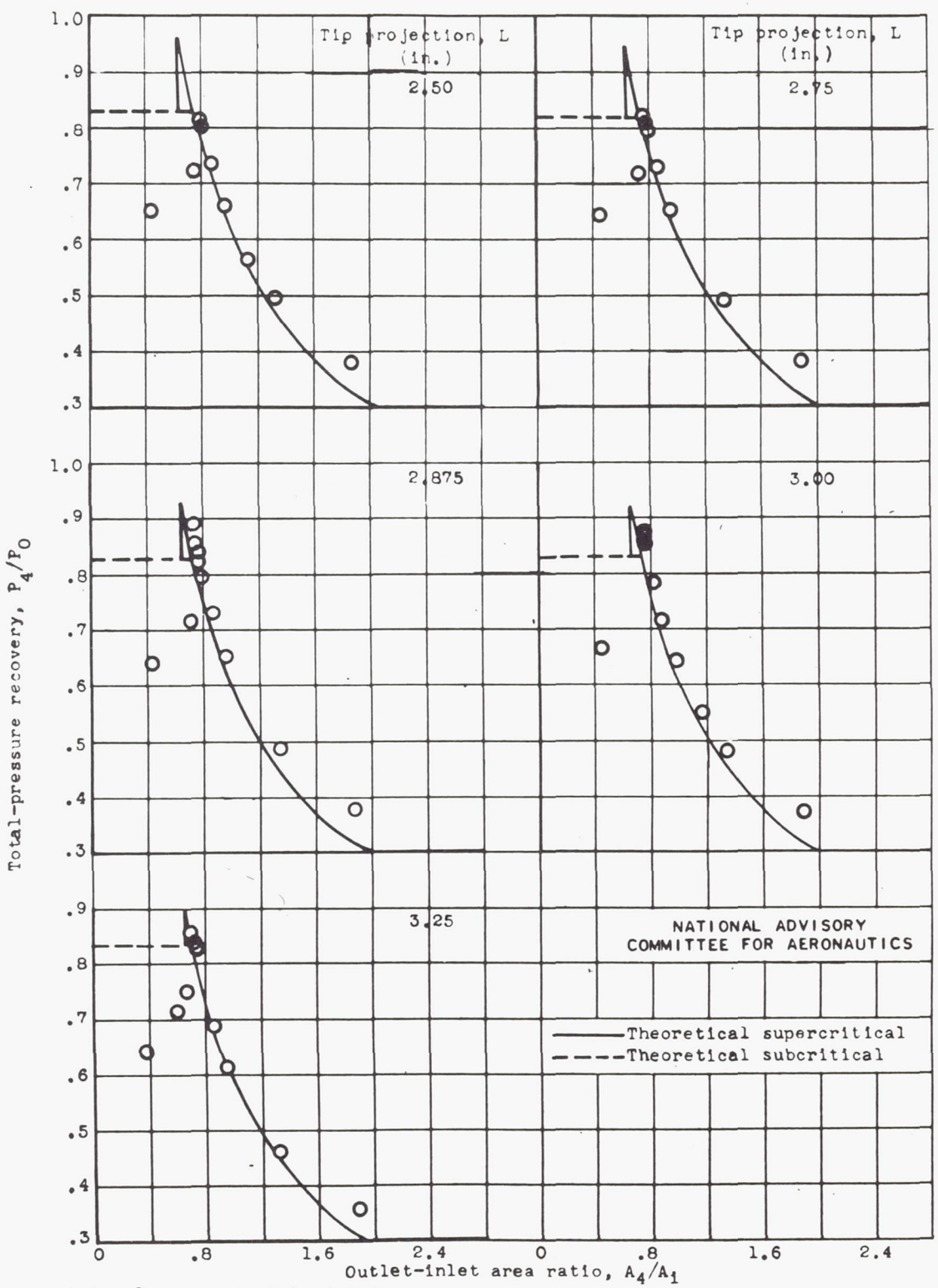

(a) 20° cone, straight inlet.

Figure 5.- Variation of total-pressure recovery with outlet-inlet area ratio at angle of attack of 0°.

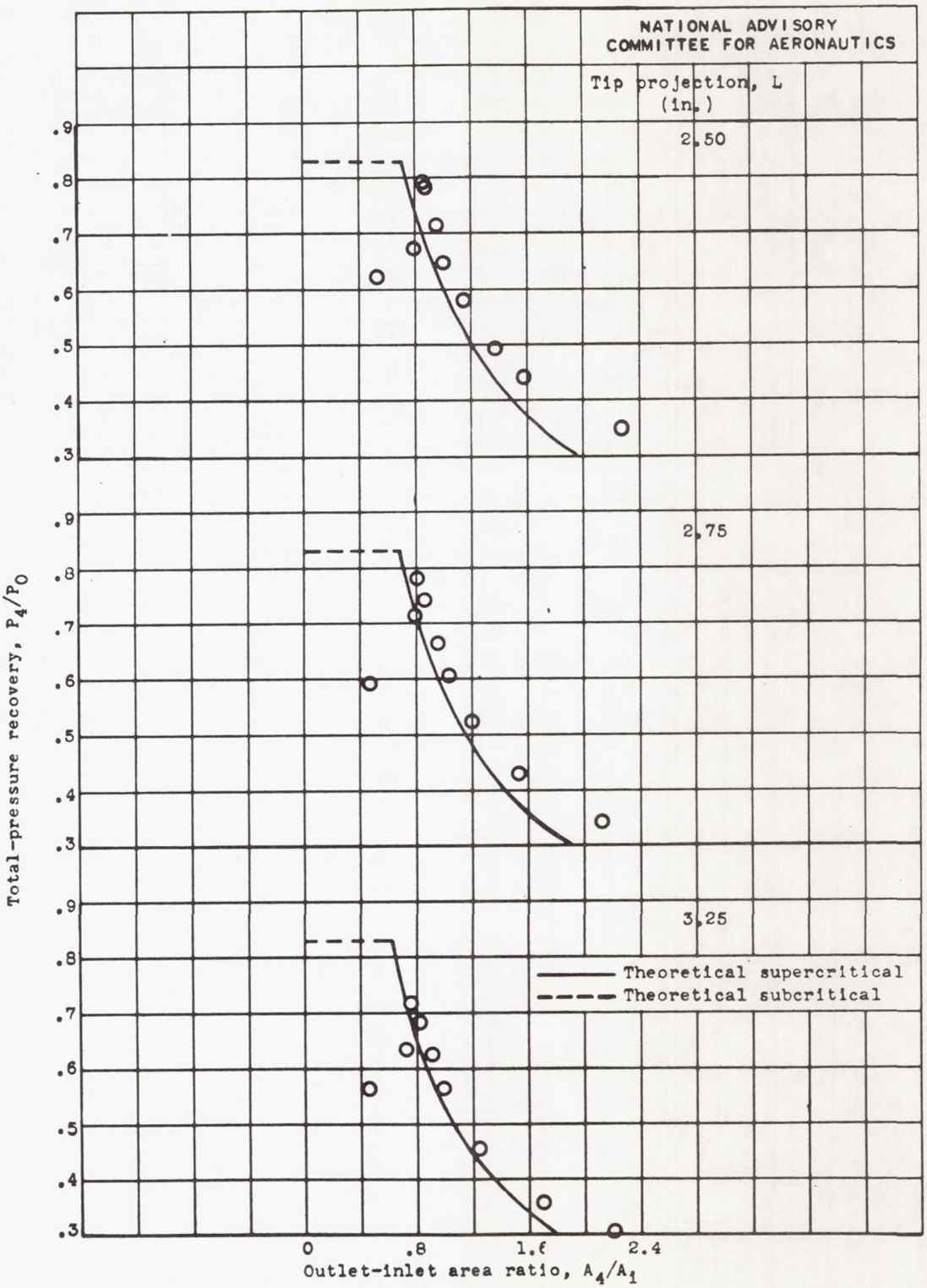

(b) 20° cone, curved inlet.

Figure 5.- Continued. Variation of total-pressure recovery with outlet-inlet area ratio at angle of attack of 0°.

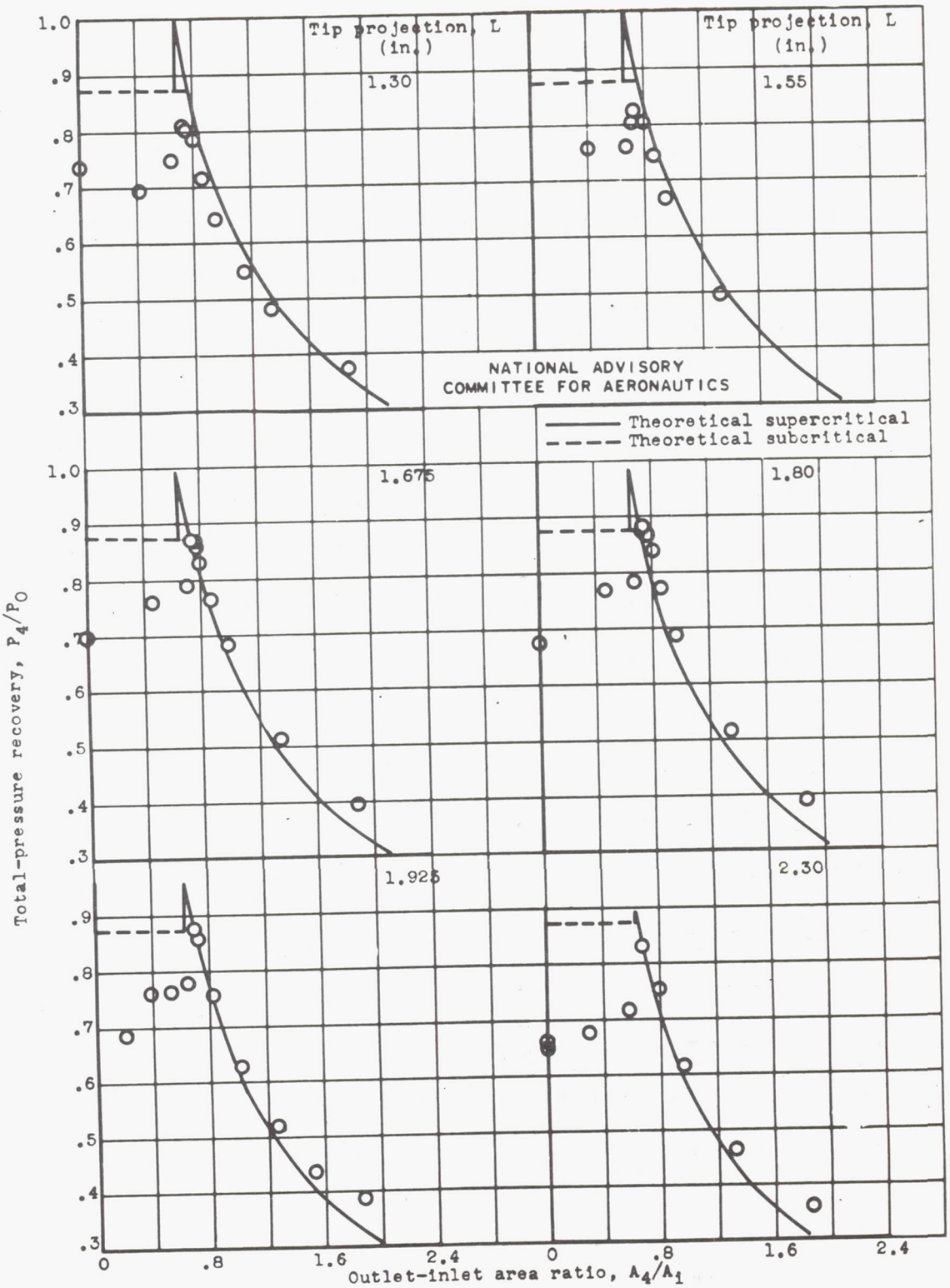

(c) 30° cone, straight inlet.

Figure 5.- Continued. Variation of total-pressure recovery with outlet-inlet area ratio at angle of attack of 0°.

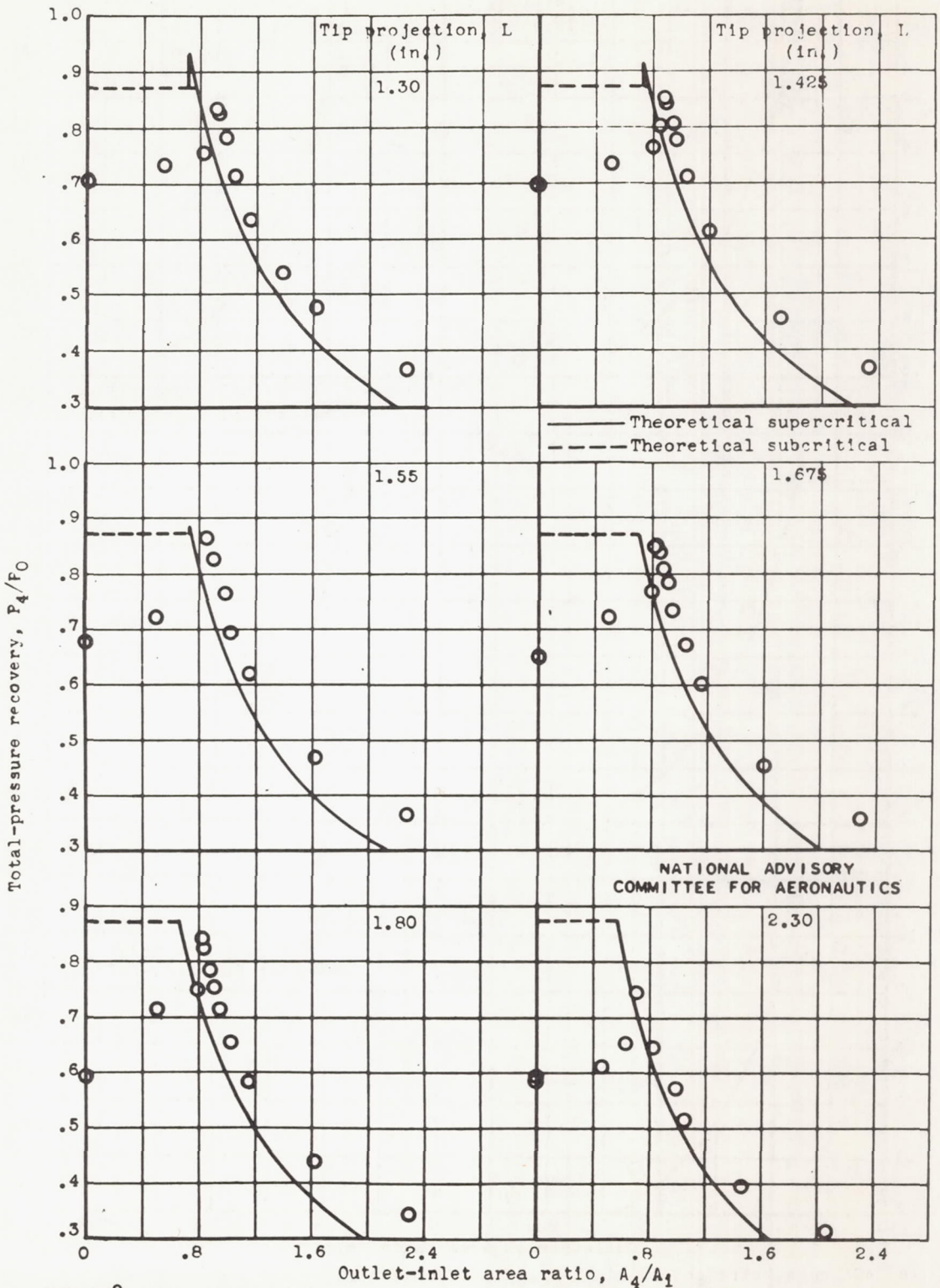

(d) 30° cone, curved inlet.

Figure 5.- Continued. Variation of total-pressure recovery with outlet-inlet area ratio at angle of attack of 0°.

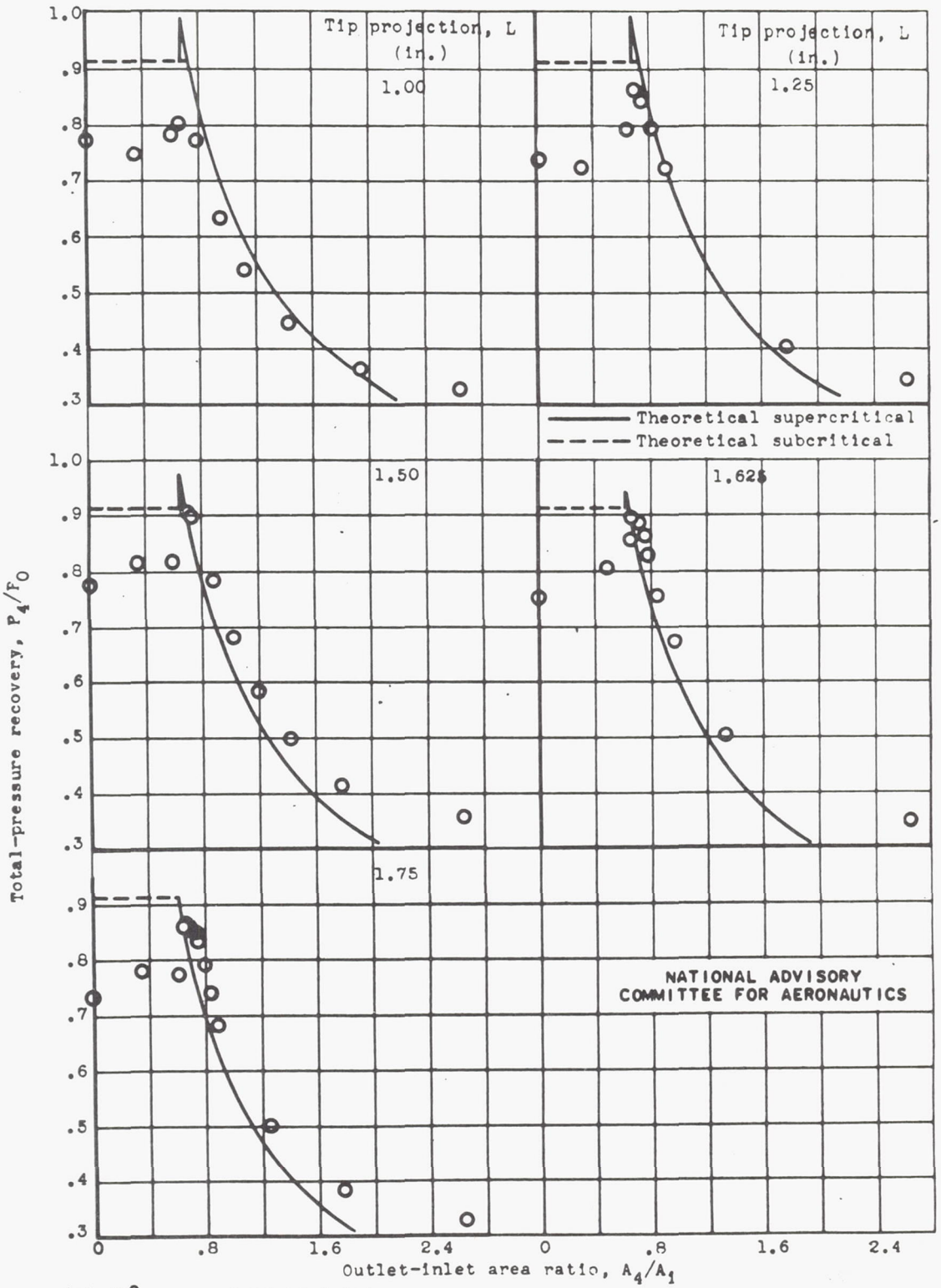

(e) 40° cone, straight inlet.

Figure 5.- Continued. Variation of total-pressure recovery with outlet-inlet area ratio at angle of attack of 0°.

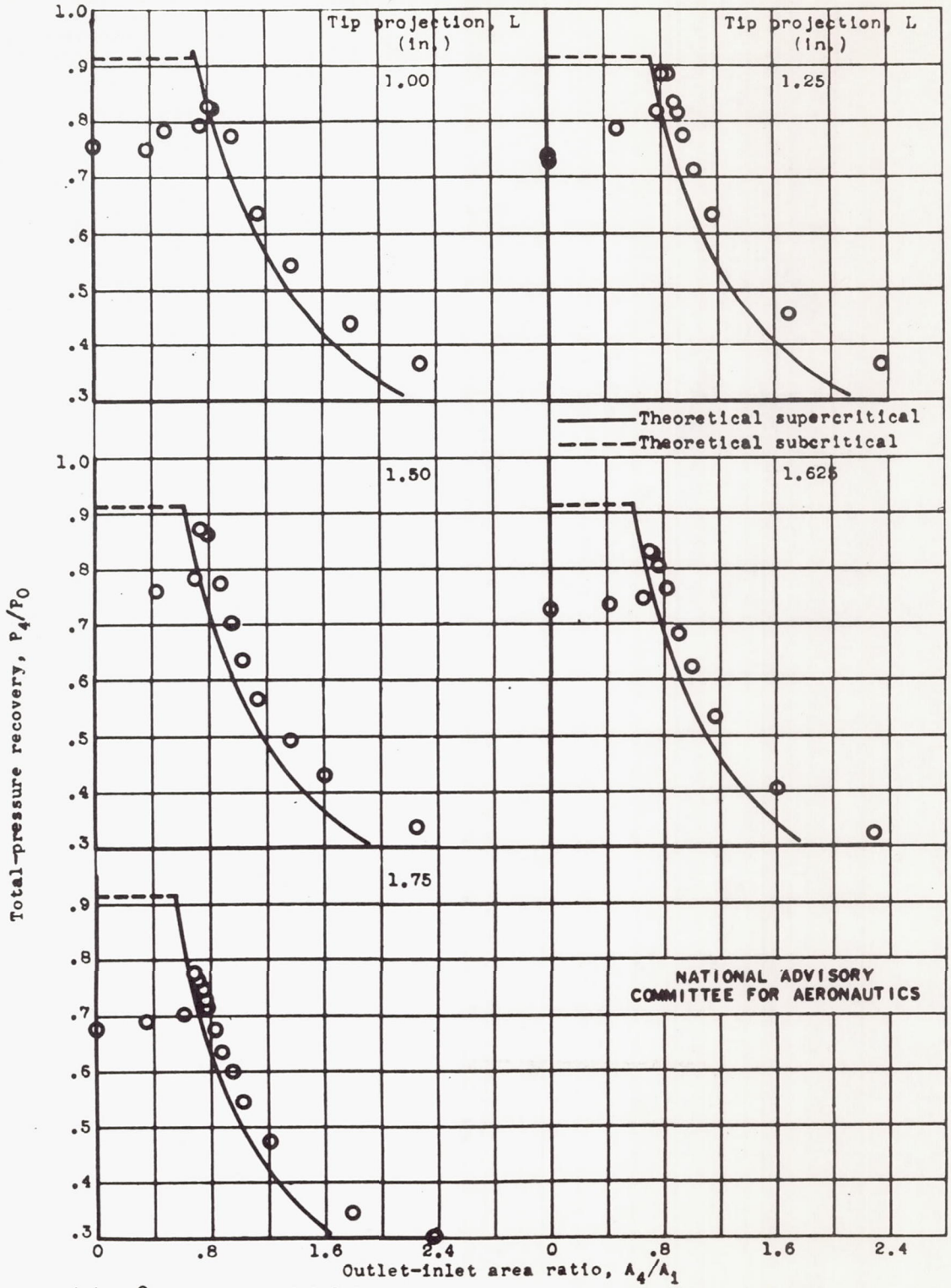

(f) 40° cone, curved inlet.

Figure 5.- Continued. Variation of total-pressure recovery with outlet-inlet area ratio at angle of attack of 0°.

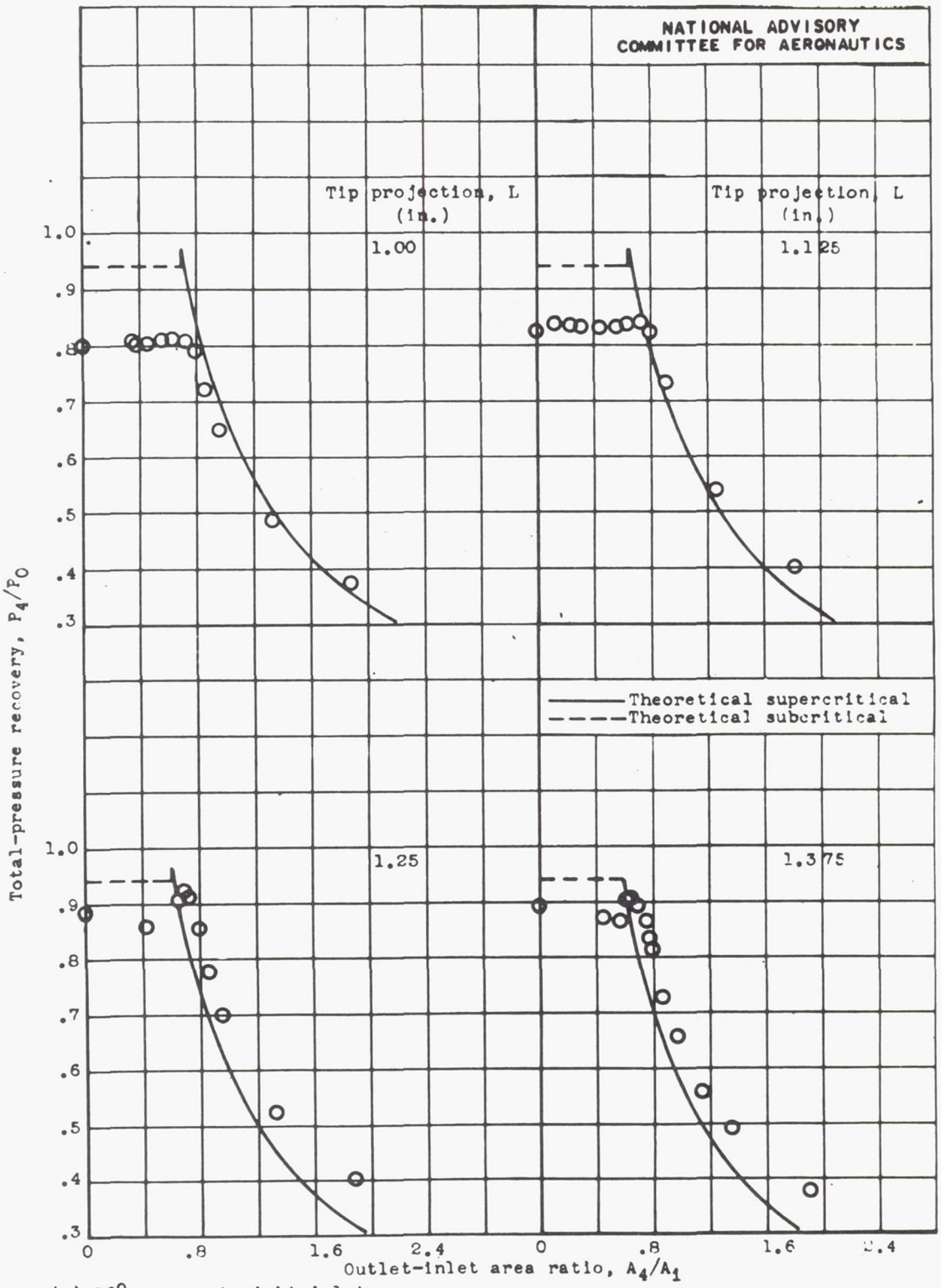

(g) 50° cone, straight inlet.

Figure 5.- Continued. Variation of total-pressure recovery with outlet-inlet area ratio at angle of attack of 0°.

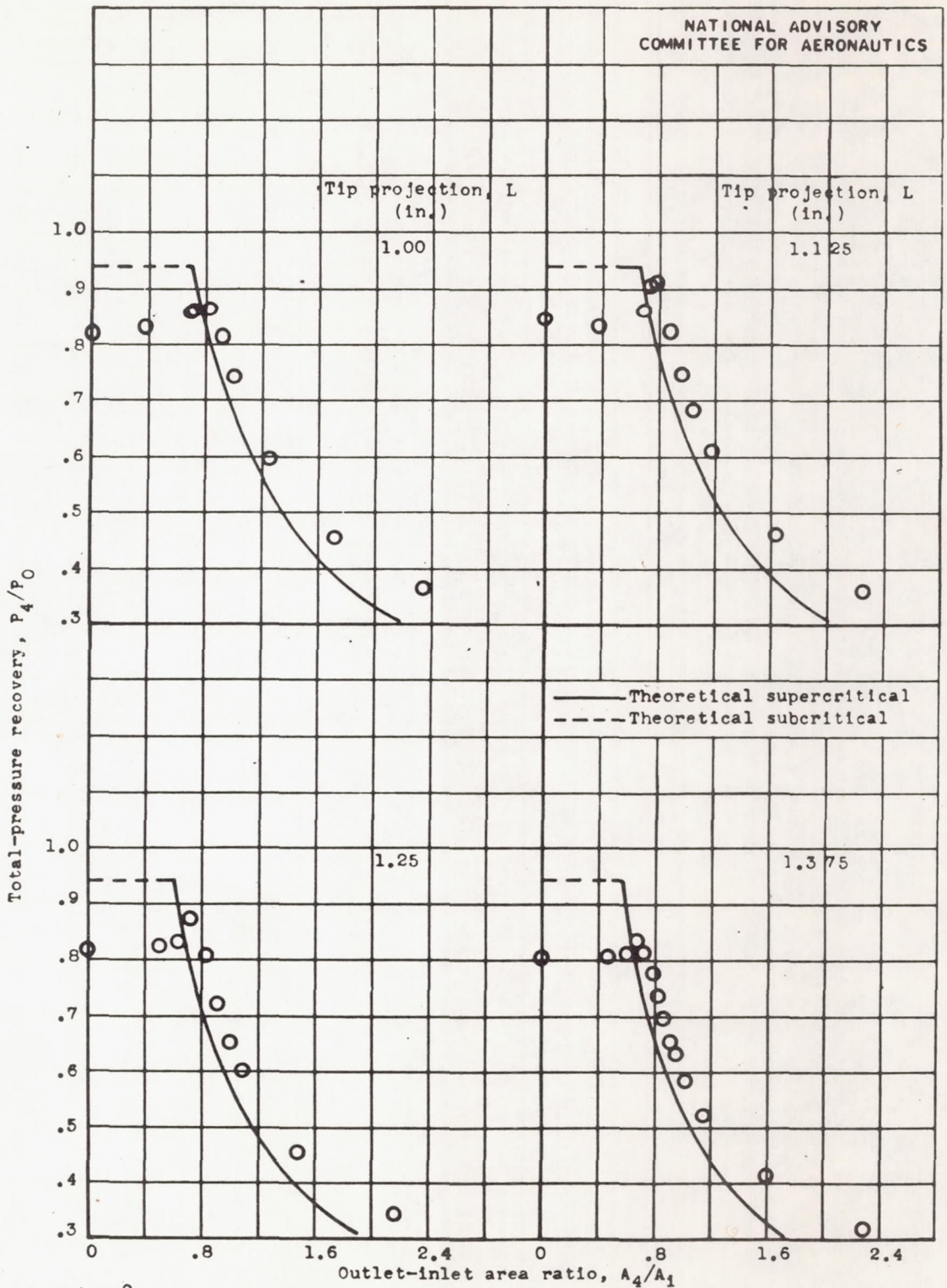

(h) 50° cone, curved inlet.

Figure 5.- Continued. Variation of total-pressure recovery with outlet-inlet area ratio at angle of attack of 0°.

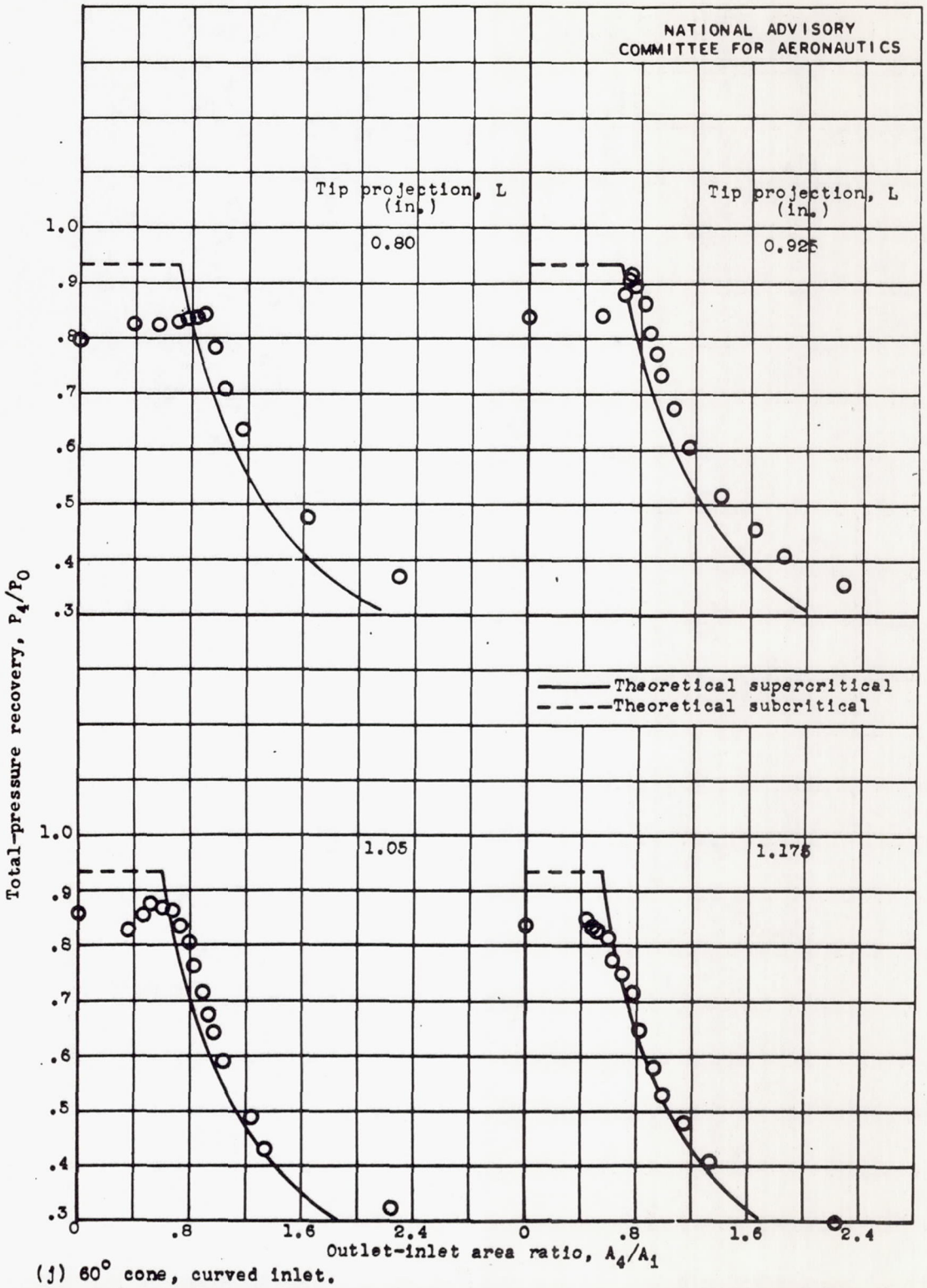

(j) 60° cone, curved inlet.

Figure 5.- Continued. Variation of total-pressure recovery with outlet-inlet area ratio at angle of attack of 0°.

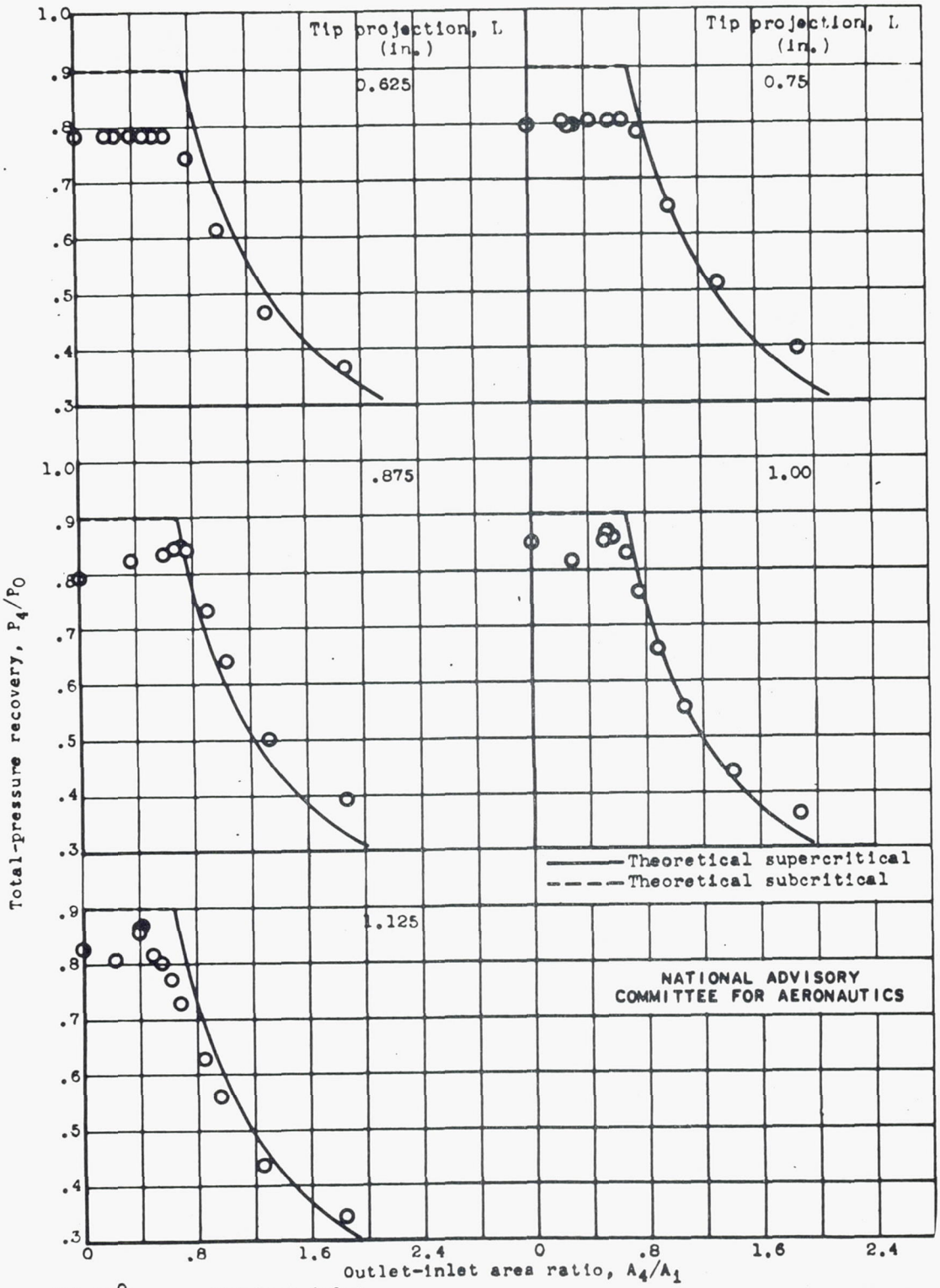

(k) 70° cone, straight inlet.

Figure 5.- Continued. Variation of total-pressure recovery with outlet-inlet area ratio at angle of attack of 0°.

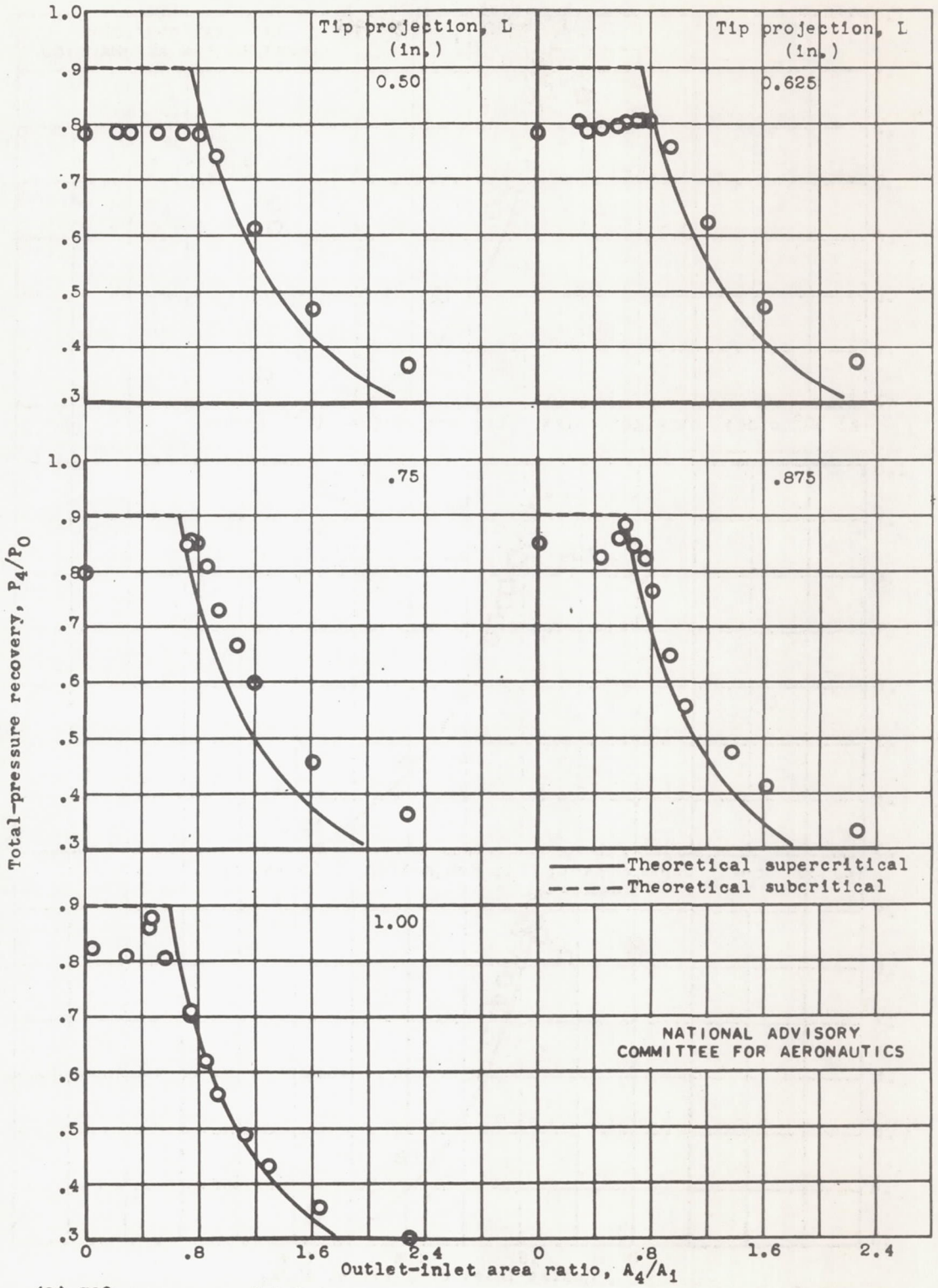

(1) 70° cone, curved inlet.

Figure 5.- Concluded. Variation of total-pressure recovery with outlet-inlet area ratio at angle of attack of 0°.

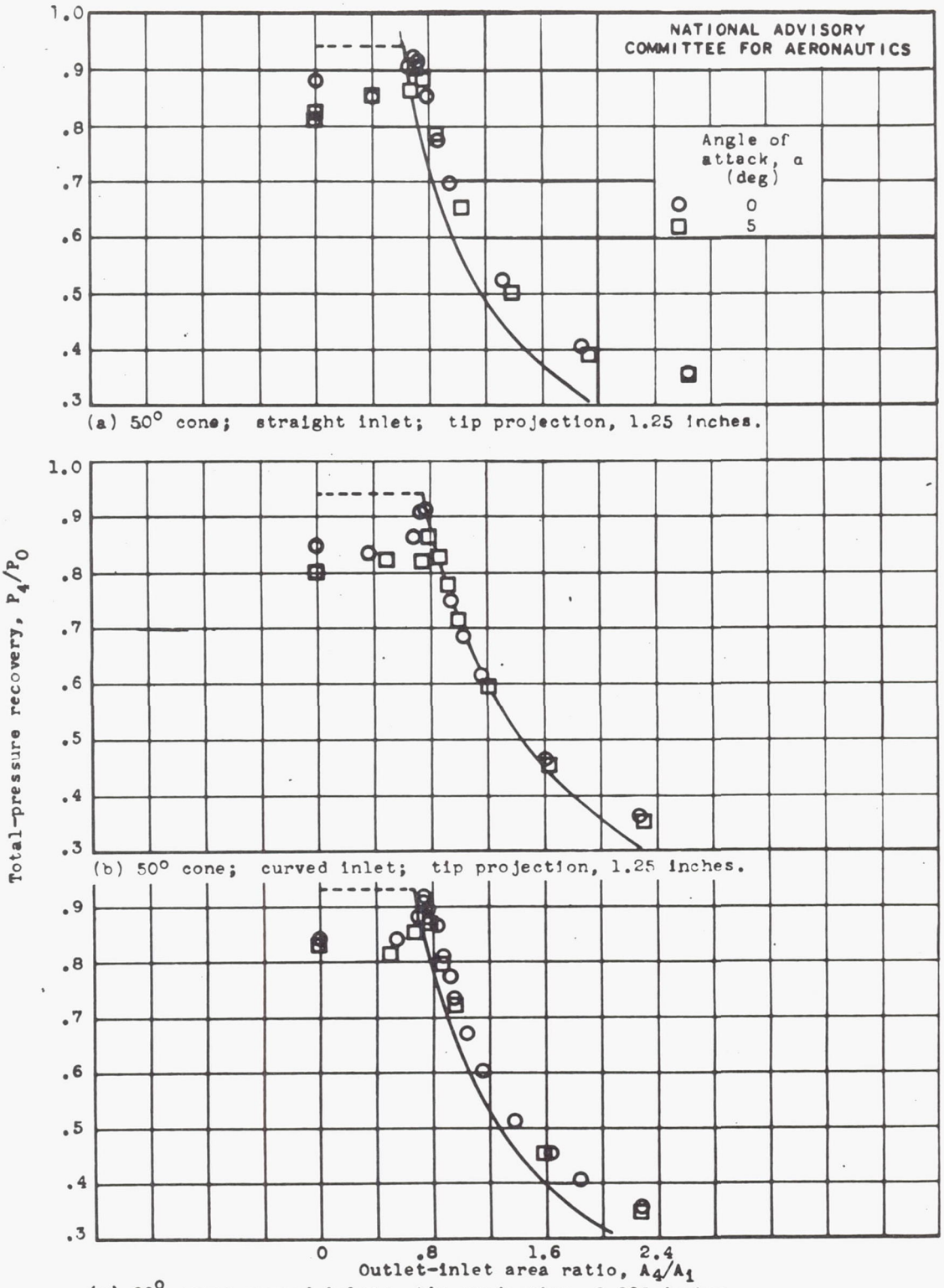

(a) 50° cone; straight inlet; tip projection, 1.25 inches.

(b) 50° cone; curved inlet; tip projection, 1.25 inches.

(c) 60° cone; curved inlet; tip projection, 0.925 inches.

Figure 6.- Effect of angle of attack on total-pressure recovery obtained with three configurations.

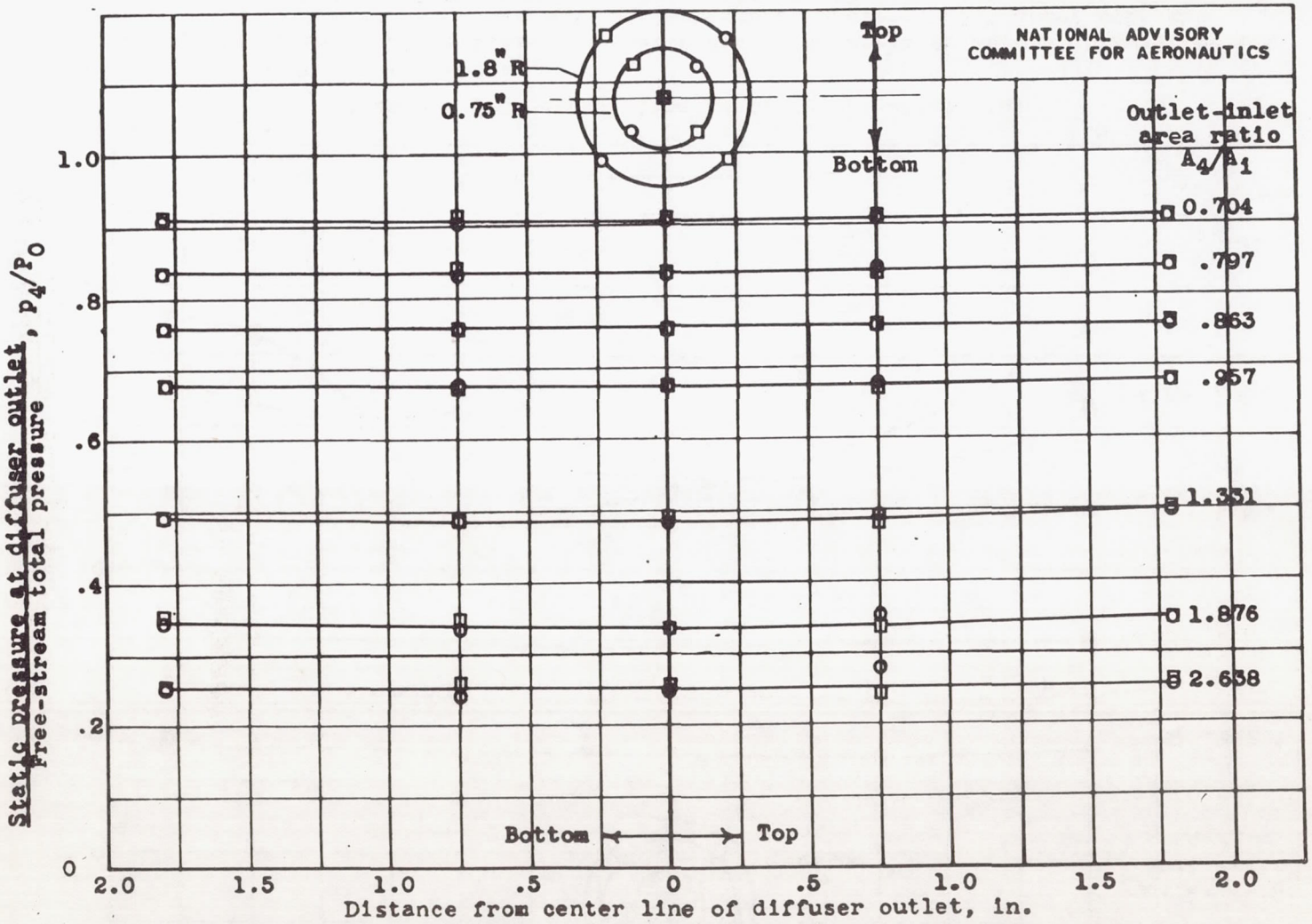

(a) Static-pressure distribution.

Figure 7.- Distribution of static and total pressure across diffuser outlet with configuration yielding maximum total-pressure recovery. 50° cone; straight inlet; tip projection, 1.25 inches; angle of attack, 0°.

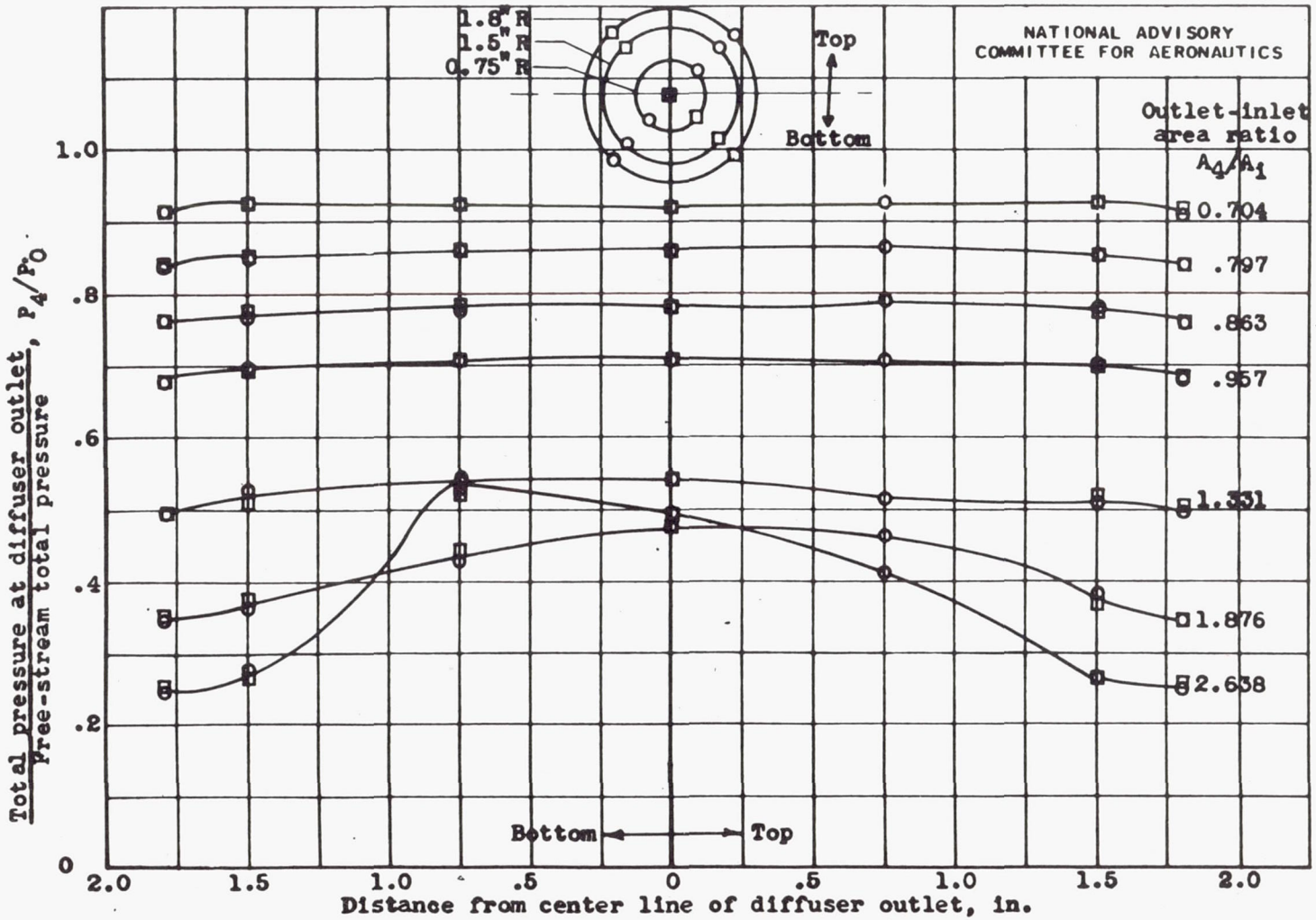

(b) Total-pressure distribution.

Figure 7.- Concluded. Distribution of static and total pressure across diffuser outlet with configuration yielding maximum total-pressure recovery. 50° cone; straight inlet; tip projection, 1.25 inches; angle of attack, 0°.

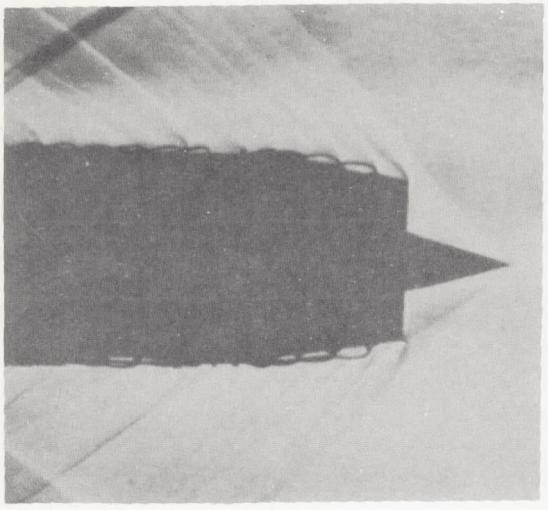

(a) Supercritical flow with tip projection less than optimum: 30° cone; straight inlet; L, 1.55 inches; A_4/A_j, 1.336; P_4/P_0, 0.495; angle of attack, 0°.

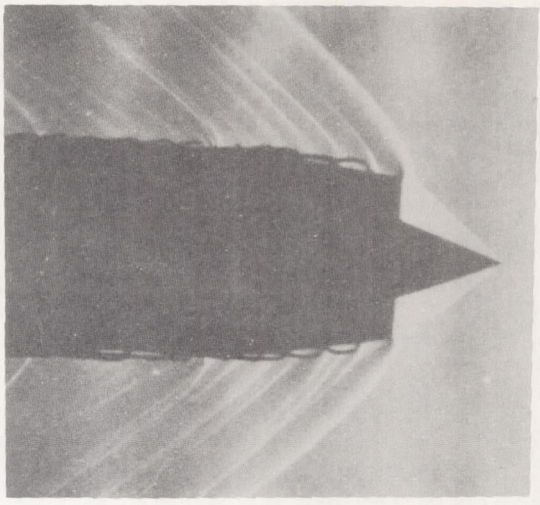

(b) Subcritical flow with optimum tip projection: 40° cone; straight inlet; L, 1.50 inches; A_4/A_j, 0.705 P_4/P_0, 0.900; angle of attack, 0°.

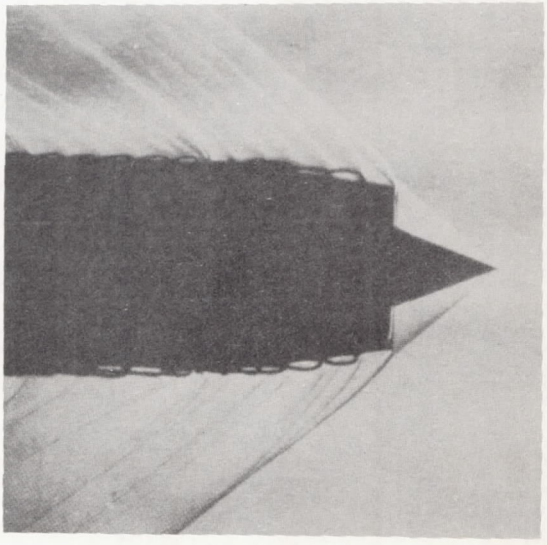

NACA
C-17176
11-8-46

(c) Supercritical flow with optimum tip projection: 40° cone; straight inlet; L, 1.50 inches; A_4/A_j, 1.410; P_4/P_0, 0.500; angle of attack, 0°.

Figure 8. - Schlieren photographs of typical flow patterns.

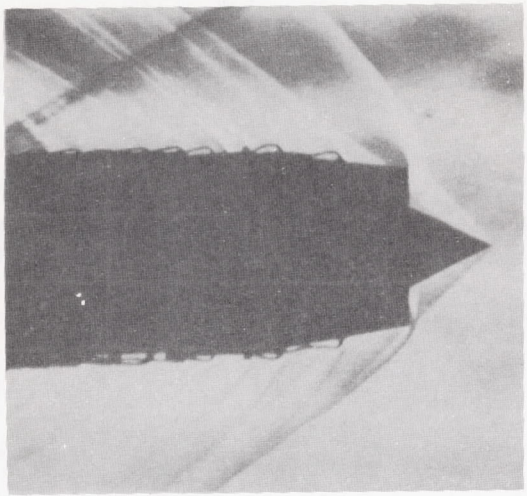

(d) Subcritical flow for highest total-pressure recovery obtained with angle of attack of 5°. 50° cone; straight inlet; L, 1.25 inches; A_4/A_i, 0.705; P_4/P_0, 0.908.

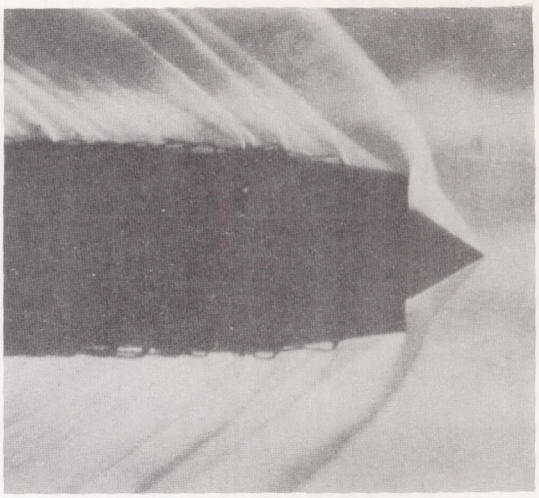

e) Subcritical flow with high total-pressure recovery: 60° cone; straight inlet; L, 1.175 inches; A_4/A_i, 0.544; P_4/P_0, 0.912; angle of attack, 0°.

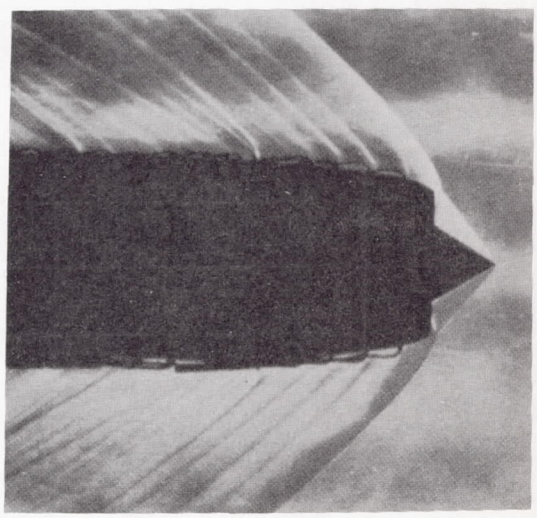

NACA
C-17177
11-8-46

(f) Subcritical flow with high total-pressure recovery: 60° cone; curved inlet; L, 0.925 inch; A_4/A_i, 0.760; P_4/P_0, 0.893; angle of attack, 0°.

Figure 8. - Concluded. Schlieren photographs of typical flow patterns.

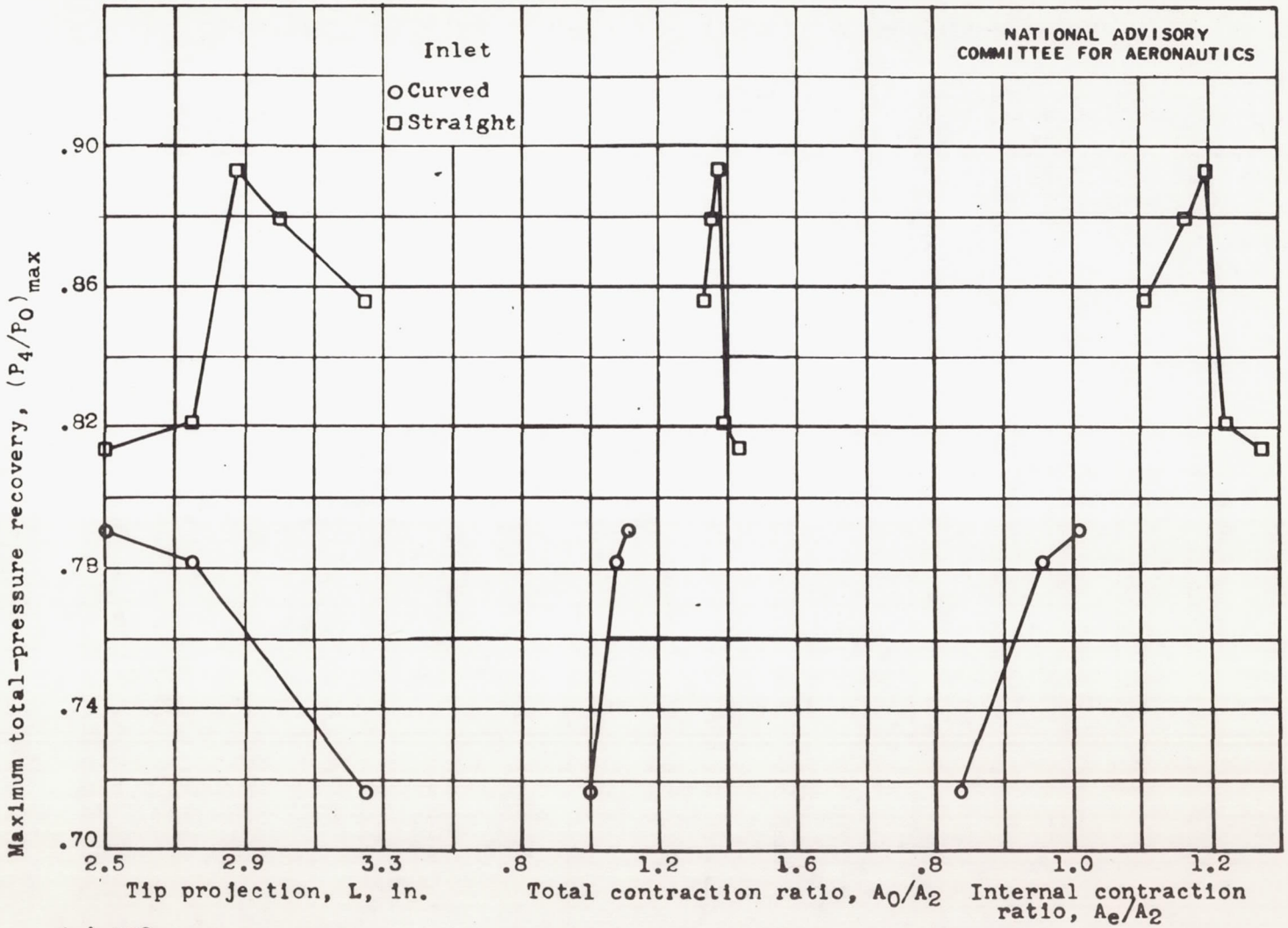

(a) 20° cone.

Figure 9.- Variation of maximum total-pressure recovery with tip projection, total contraction ratio, and internal contraction ratio.

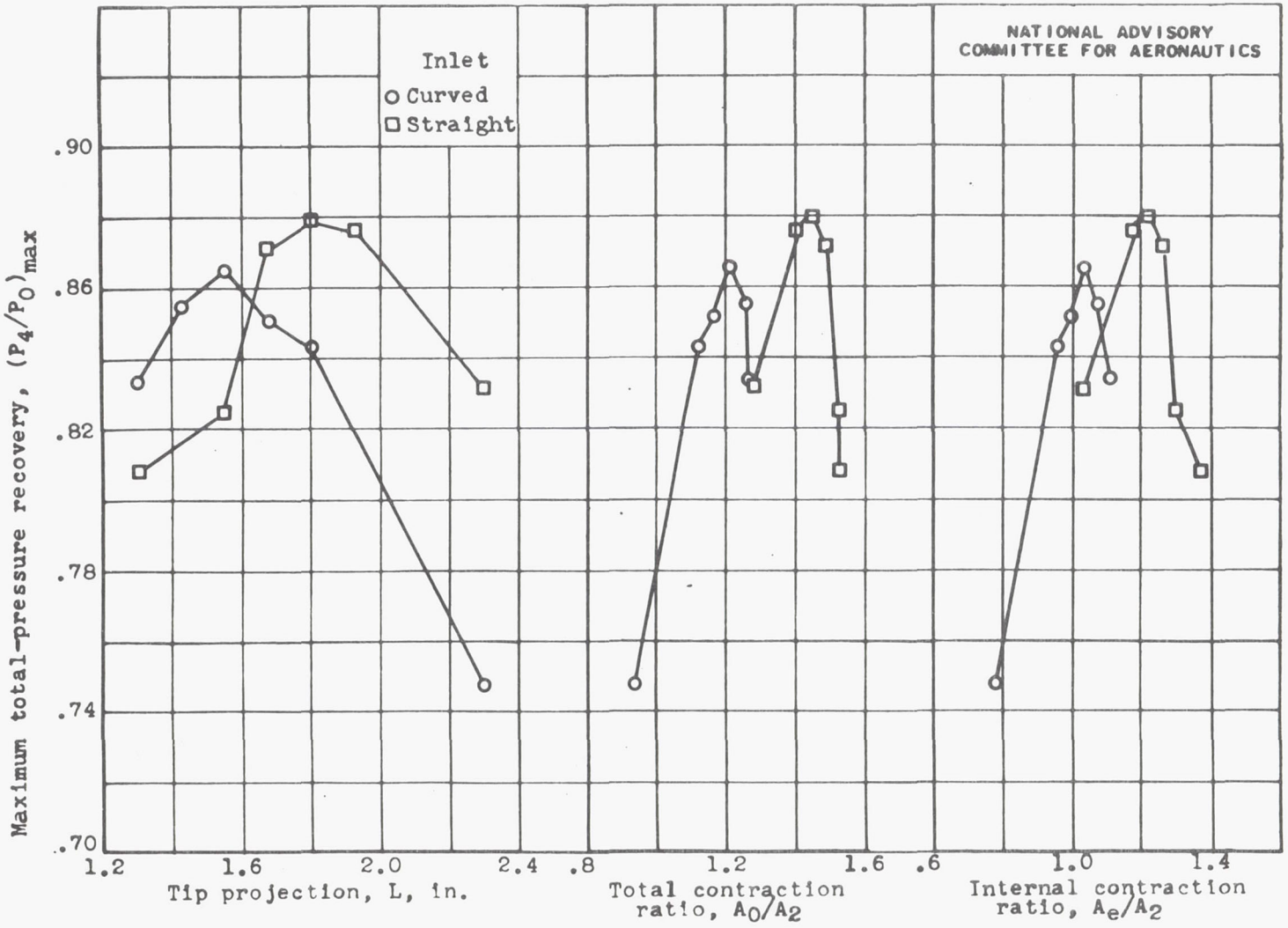

(b) 30° cone.

Figure 9.- Continued. Variation of maximum total-pressure recovery with tip projection, total contraction ratio, and internal contraction ratio.

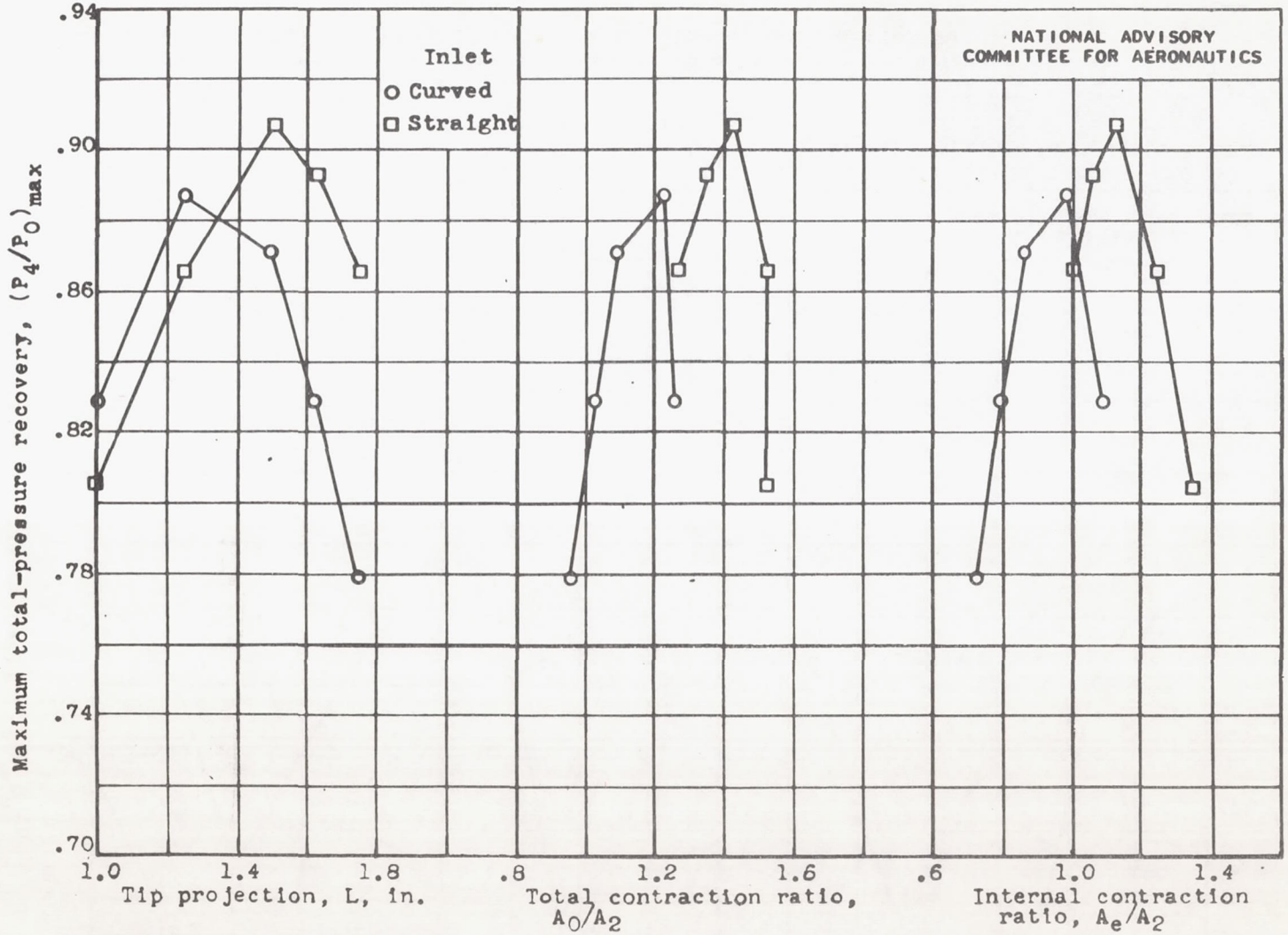

(c) 40° cone.

Figure 9.- Continued. Variation of maximum total-pressure recovery with tip projection, total contraction ratio, and internal contraction ratio.

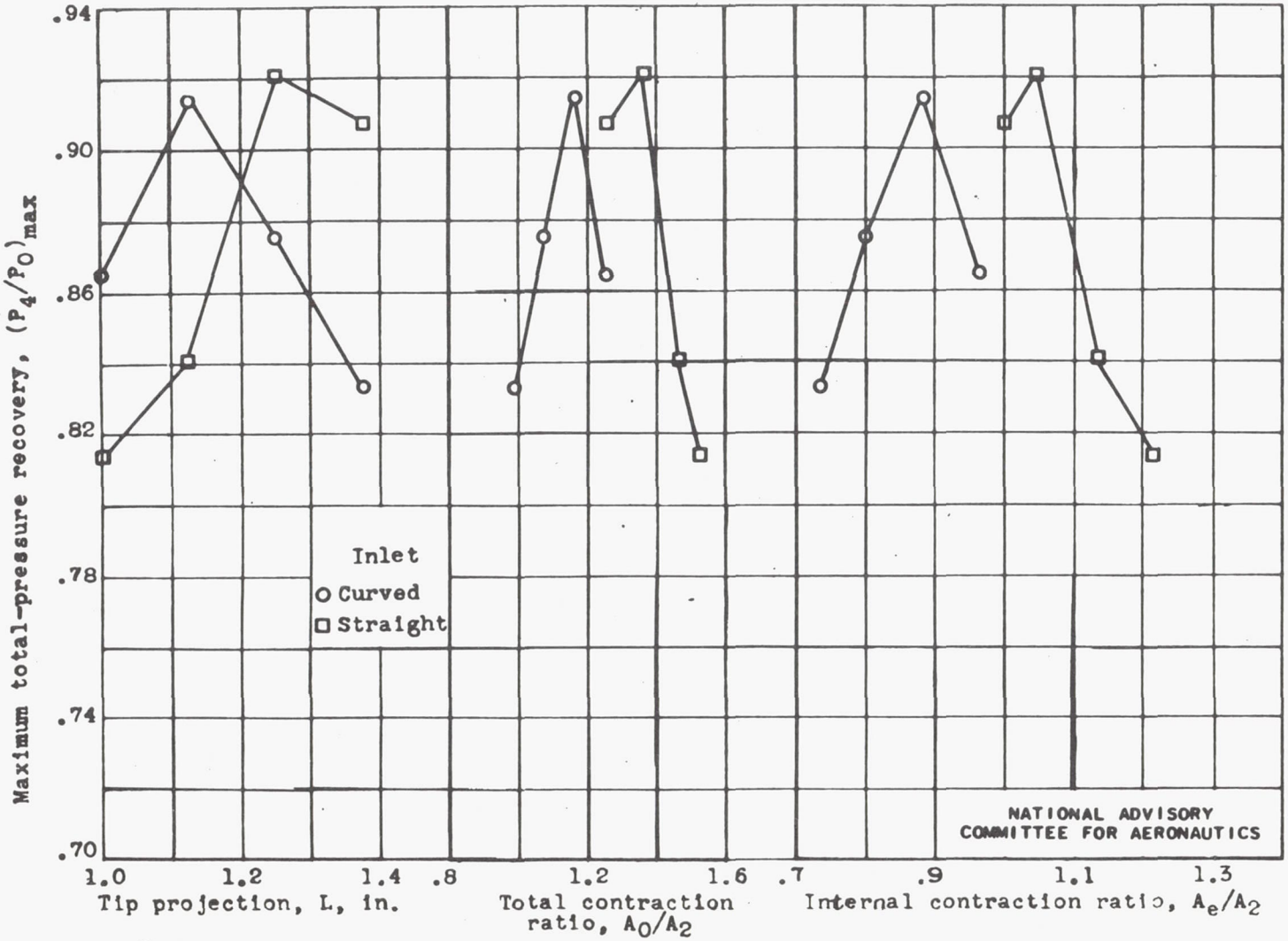

(d) 50° cone.

Figure 9.- Continued. Variation of maximum total-pressure recovery with tip projection, total contraction ratio, and internal contraction ratio.

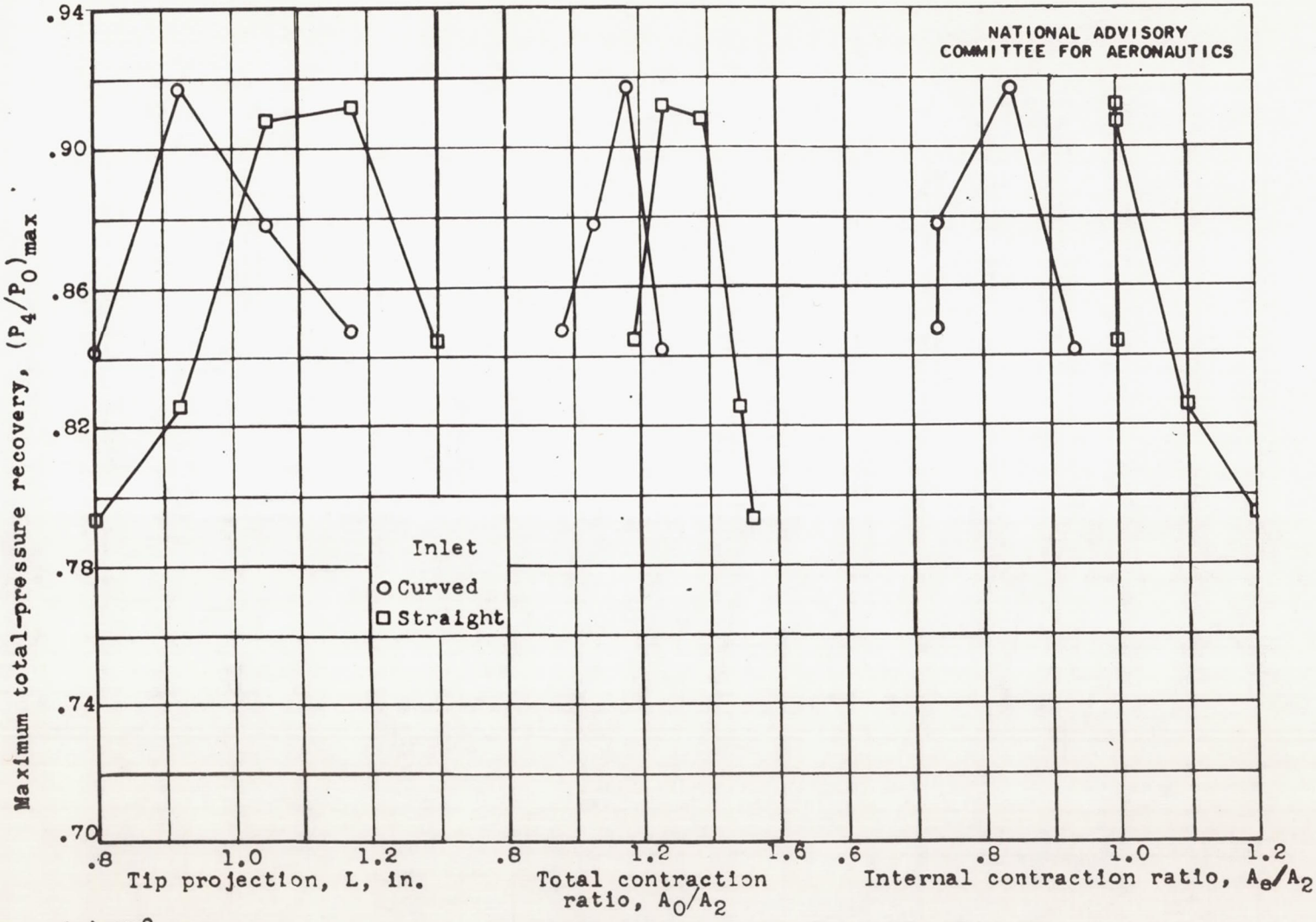

(e) 60° cone.

Figure 9.- Continued. Variation of maximum total-pressure recovery with tip projection, total contraction ratio, and internal contraction ratio.

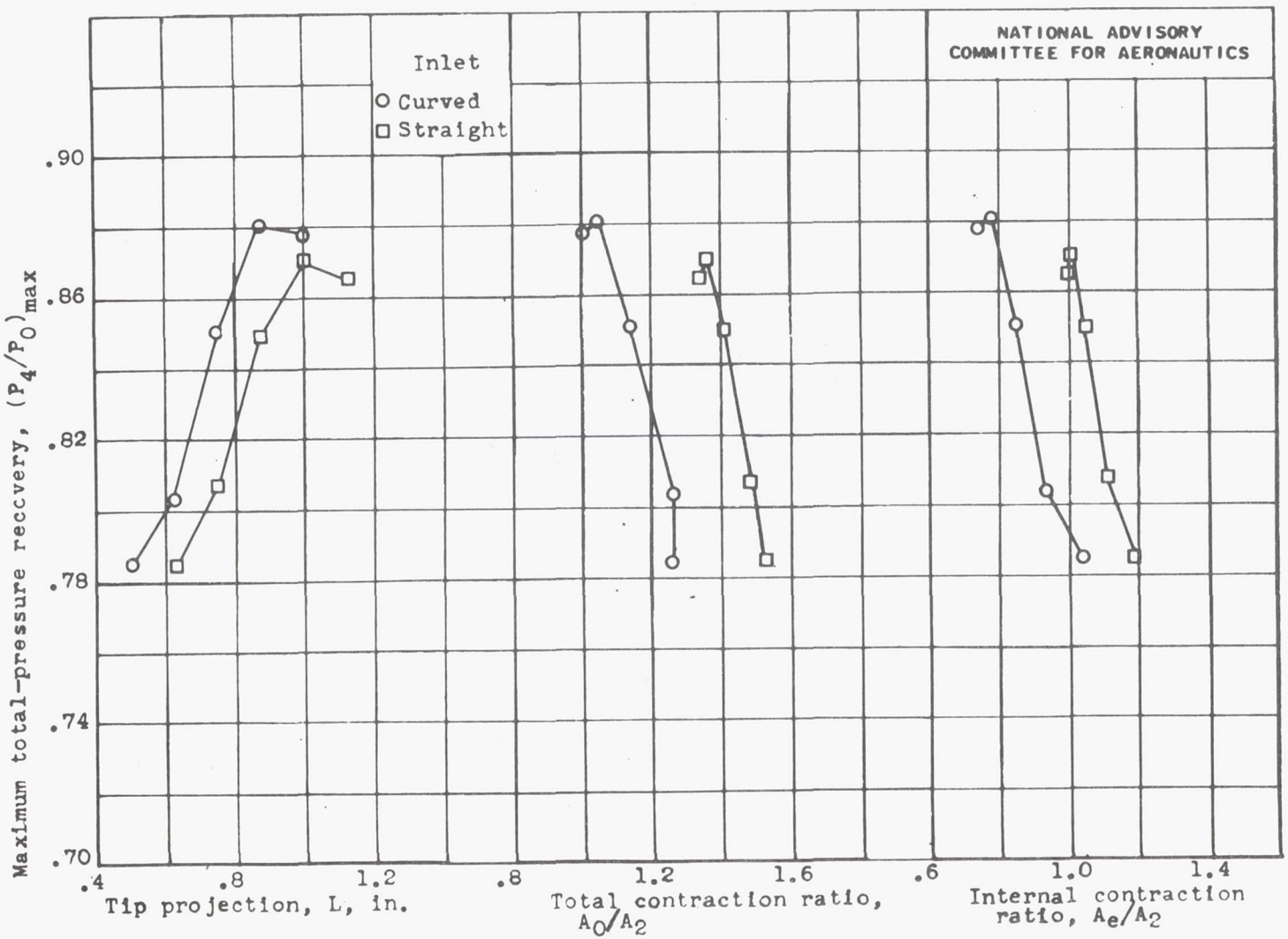

(f) 70° cone.

Figure 9.- Concluded. Variation of maximum total-pressure recovery with tip projection, total contraction ratio, and internal contraction ratio.

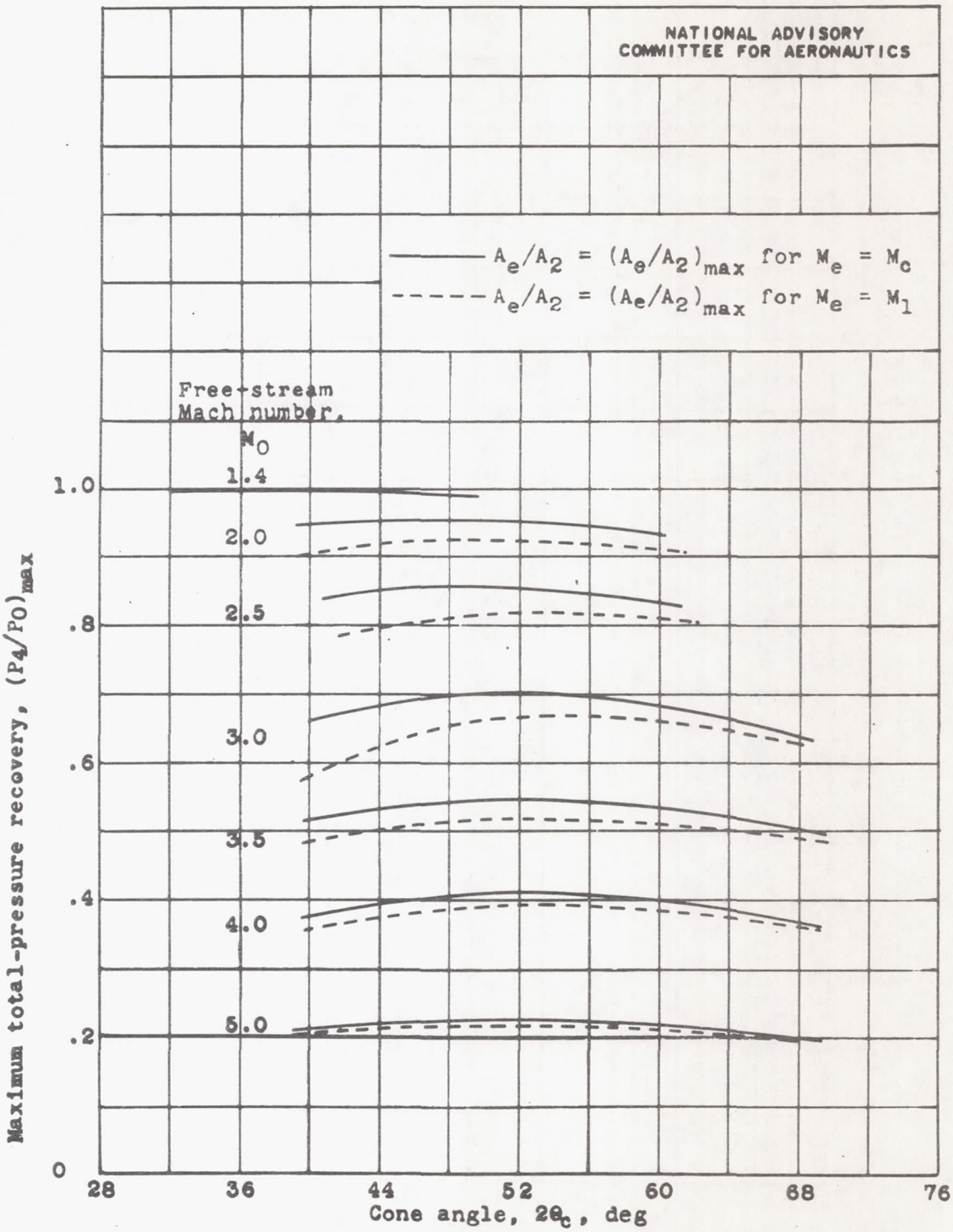

Figure 10.- Variation of maximum theoretical total-pressure recovery of single-shock diffuser with cone angle for various Mach numbers.

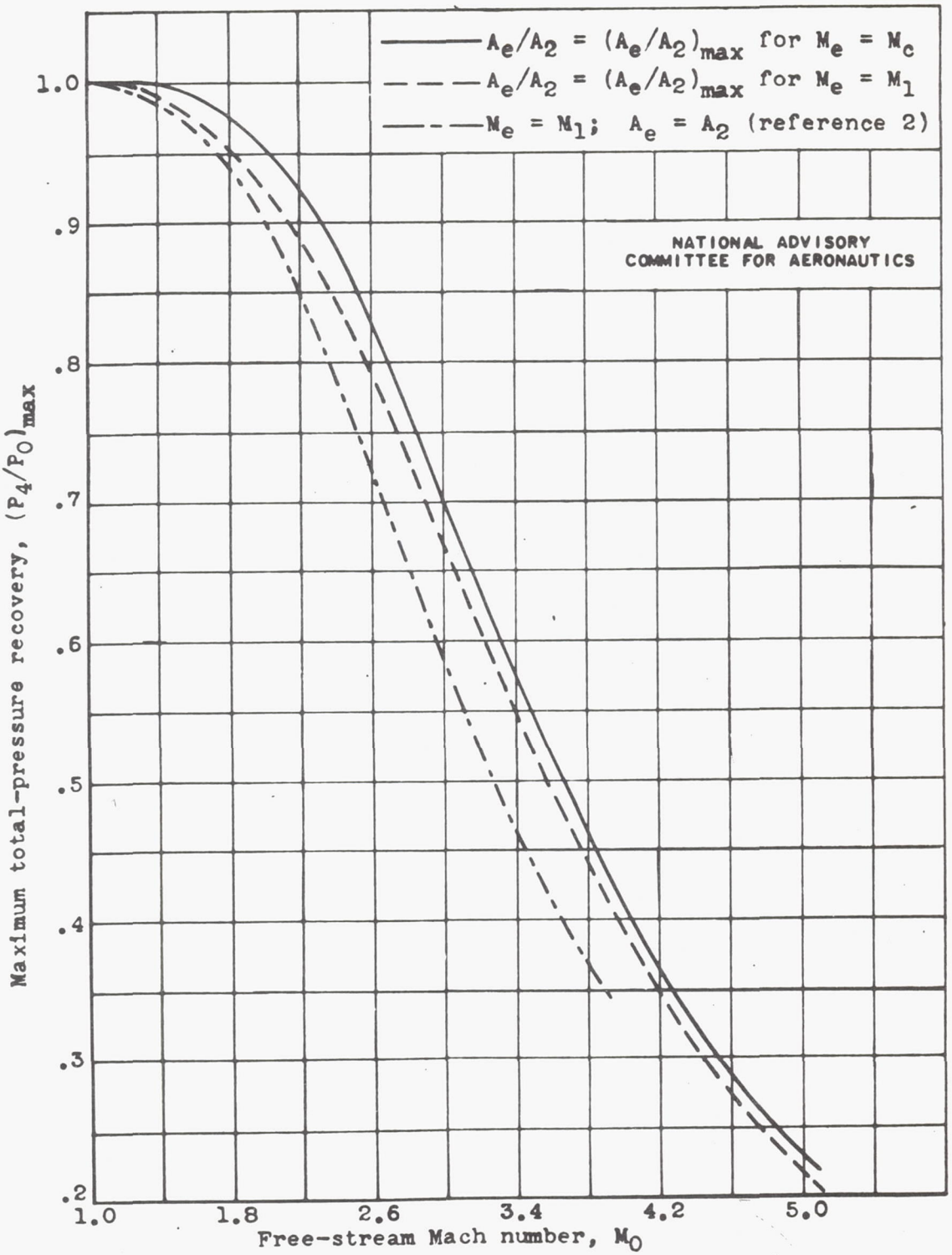

Figure 11.- Variation of maximum theoretical total-pressure recovery of single-shock diffuser with Mach number for several assumptions.

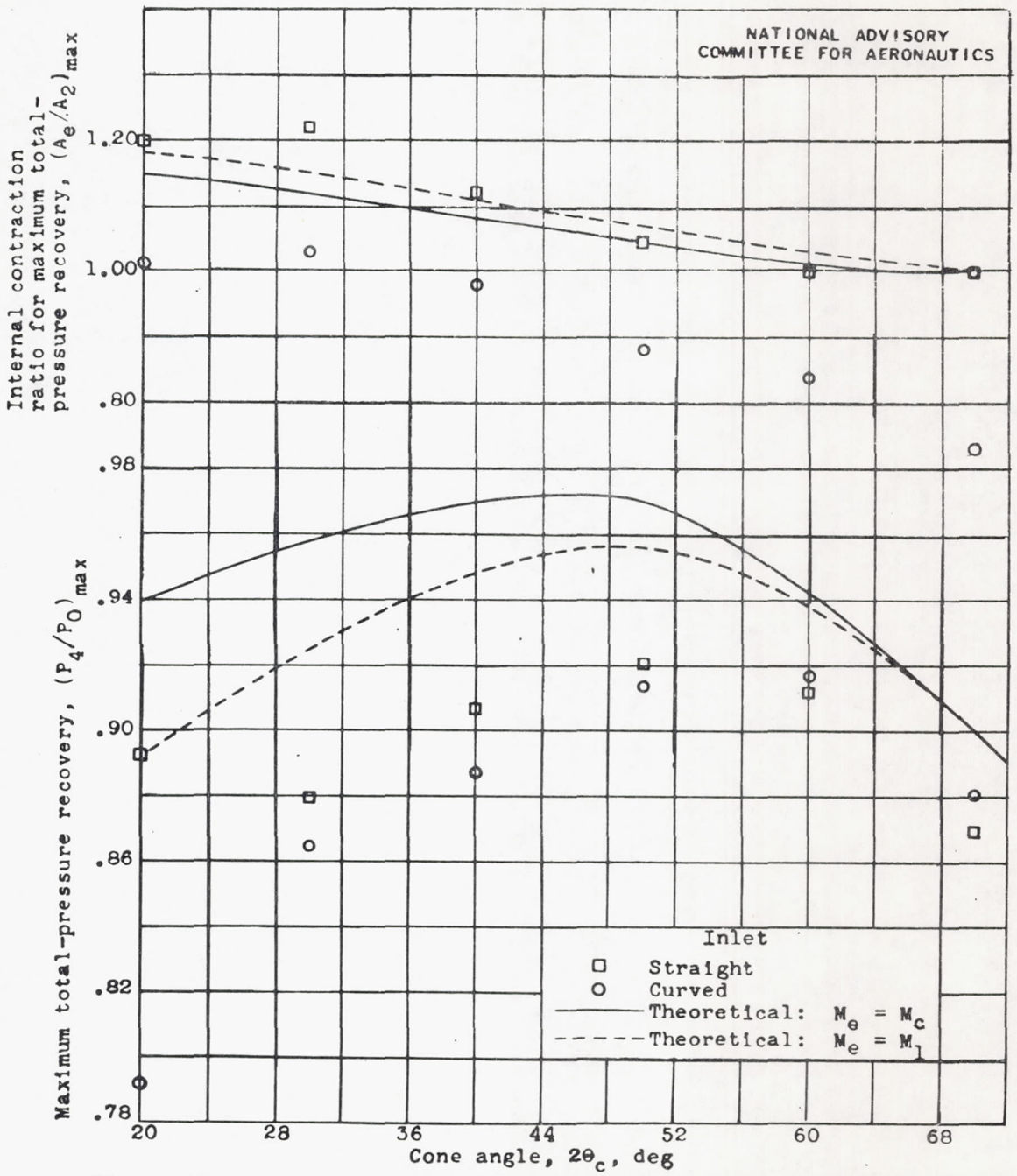

Figure 12.- Variation of maximum theoretical and experimental total-pressure recovery and internal contraction ratio with cone angle.